SHALE OIL PRODUCTION PERFORMANCE FROM A STIMULATED RESERVOIR VOLUME

A Thesis

by

ANISH SINGH CHAUDHARY

Submitted to the Office of Graduate Studies of
Texas A&M University
in fulfillment of the requirements for the degree of

MASTER OF SCIENCE

August 2011

Major Subject: Petroleum Engineering

Shale Oil Production Performance from a Stimulated Reservoir Volume

SHALE OIL PRODUCTION PERFORMANCE FROM A STIMULATED RESERVOIR VOLUME

A Thesis

by

ANISH SINGH CHAUDHARY

Submitted to the Office of Graduate Studies of
Texas A&M University
in partial fulfillment of the requirements for the degree of

MASTER OF SCIENCE

Approved by:

Chair of Committee,	Christine Ehlig-Economides
Committee Members,	Robert A. Wattenbarger
	Maria A. Barrufet
Head of Department,	Stephen A. Holditch

August 2011

Major Subject: Petroleum Engineering

ABSTRACT

Shale Oil Production Performance from a Stimulated Reservoir Volume.

(August 2011)

Anish Singh Chaudhary, B.Tech, Indian School of Mines, Dhanbad

Chair of Advisory Committee: Dr. Christine Ehlig-Economides

The horizontal well with multiple transverse fractures has proven to be an effective strategy for shale gas reservoir exploitation. Some operators are successfully producing shale oil using the same strategy. Due to its higher viscosity and eventual 2-phase flow conditions when the formation pressure drops below the oil bubble point pressure, shale oil is likely to be limited to lower recovery efficiency than shale gas. However, the recently discovered Eagle Ford shale formations is significantly over pressured, and initial formation pressure is well above the bubble point pressure in the oil window. This, coupled with successful hydraulic fracturing methodologies, is leading to commercial wells. This study evaluates the recovery potential for oil produced both above and below the bubble point pressure from very low permeability unconventional shale oil formations.

We explain how the Eagle Ford shale is different from other shales such as the Barnett and others. Although, Eagle Ford shale produces oil, condensate and dry gas in different areas, our study focuses in the oil window of the Eagle Ford shale. We used the logarithmically gridded locally refined gridding scheme to properly model the flow in the hydraulic fracture, the flow from the fracture to the matrix and the flow in the matrix.

The steep pressure and saturation changes near the hydraulic fractures are captured using this gridding scheme. We compare the modeled production of shale oil from the very low permeability reservoir to conventional reservoir flow behavior.

We show how production behavior and recovery of oil from the low permeability shale formation is a function of the rock properties, formation fluid properties and the fracturing operations. The sensitivity studies illustrate the important parameters affecting shale oil production performance from the stimulated reservoir volume. The parameters studied in our work includes fracture spacing, fracture half-length, rock compressibility, critical gas saturation (for 2 phase flow below the bubble point of oil), flowing bottom-hole pressure, hydraulic fracture conductivity, and matrix permeability.

The sensitivity studies show that placing fractures closely, increasing the fracture half-length, making higher conductive fractures leads to higher recovery of oil. Also, the thesis stresses the need to carry out the core analysis and other reservoir studies to capture the important rock and fluid parameters like the rock permeability and the critical gas saturation.

DEDICATION

To my mother and father

ACKNOWLEDGEMENTS

I would like to thank my committee chair, Dr. Christine Ehlig-Economides, and my committee members, Dr. Robert A. Wattenbarger, and Dr. Maria A. Barrufet, for their guidance and support throughout the course of this research.

Thanks also go to my friends and colleagues and the department faculty and staff for making my time at Texas A&M University a great experience. I also want to extend my gratitude to the Computer Modeling Group (CMG), for providing the Texas A&M students to work on their software.

Finally, thanks to my mother and father for their encouragement and to my friends for their patience and love.

NOMENCLATURE

AEO	Annual energy outlook
BHN	Brinell hardness number
c_f	Rock compressibility, psi-1
c_t	Total compressibility, psi-1
c_o	Oil compressibility, psi-1
C_{fD}	Dimensionless conductivity
c_w	Water Compressibility, psi-1
ft	Feet
EIA	Energy information administration
FBHP	Flowing bottom-hole pressure
GOR	Gas oil ratio
k	Formation permeability
k_f	Fracture permeability
k_{rg} at S_{org}	Relative permeability to gas at residual oil saturation to gas
N_o	Corey oil exponent
N_g	Corey gas exponent
RF	Recovery factor at 30 years, percent
S_o	Oil saturation, fraction
S_{org}	Residual oil saturation at connate gas saturation, fraction
S_{gc}	Critical gas saturation, fraction
S_w	Water saturation, fraction

SRV	Stimulated reservoir volume
PVT	Pressure volume temperature
W	Fracture width
WTI	West Texas intermediate
x_f	Fracture half-length
YM	Young's modulus

TABLE OF CONTENTS

Page

Page

LIST OF FIGURES

Page

Page

LIST OF TABLES

Page

CHAPTER I

INTRODUCTION

We begin with a brief introduction of unconventional resources/reservoirs with emphasis on development of the shale gas resources in the United States. Then we discuss the very recent phenomenon in development of the shale oil plays. Finally, we explain the objective of the current study and describe the organization of the other chapters of the thesis.

1.1 Unconventional resources

Unconventional reservoirs have been defined as formations that cannot be produced at economic flow rates or that do not produce economic volumes of oil and gas without stimulation treatments or special recovery processes and technologies (Miskimins, 2008). Typical unconventional reservoirs are tight-gas sands, coalbed methane, heavy oil, shale gas and shale oil.

On the other hand, conventional reservoirs can be produced at economic flow rates and produce economic volumes of oil and gas without large stimulation treatments or any special recovery process. Conventional reservoirs are essentially high-to medium-permeability reservoirs in which one can drill a vertical well, perforate the pay interval, and then produce the well at commercial flow rates and recover economic volumes of oil and gas (Holditch, 2002).

This thesis follows the style of *Society of Petroleum Engineers (SPE)*.

Master's, J.A. (1979) published the concept of the resource triangle, which says that oil and gas resources are distributed log normally in nature, just like any other natural resource, such as gold, copper and uranium. **Figure 1** presents the concept of the resource triangle for conventional oil and gas and for unconventional shale oil and resources. The top of the resource triangle has the conventional reservoirs which are normally small in size, easy to develop, but often difficult to find. At the bottom of the resource triangle are the unconventional reservoirs with large volumes of oil or gas in place that are generally much more difficult to develop. To produce these unconventional reservoirs, increased oil and gas prices and/or improved technology are required. Because of the log-normal distribution of natural resources, the volumes of oil and gas that are stored in these unconventional reservoirs are substantially higher than the volumes of oil and gas found in conventional reservoirs.

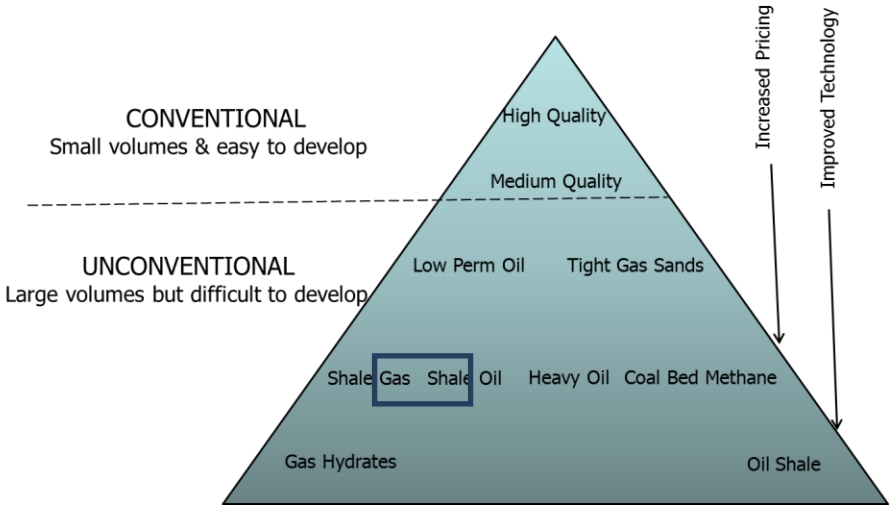

Figure 1: Resource triangle (modified from Masters, 1979)

The recent Annual Energy Outlook 2011 (AEO) from the U.S. Dept. of Energy's Energy Information Administration (EIA 2011) highlights the importance of unconventional shale gas and shale oil production in the U.S. domestic oil and gas production. **Figure 2**, from the AEO 2011, shows the natural gas production from 1990-2035. The figure shows that while total domestic natural gas production grows from 21.0 tcf in 2009 to 26.3 tcf in 2035, shale gas production grows to 12.2 trillion cubic feet in 2035, when it makes up 47 percent of total U.S. production—up considerably from the 16-percent share in 2009.

The production of shale gas has grown exponentially from year 2000 onwards. During 2000 to 2006, production of natural gas from shale gas in the United States grew by an average of 17 percent per year. Early successes in shale gas production occurred primarily in the Barnett Shale of north central Texas. By 2006, successful shale gas operations in the Barnett shale, improvements in shale gas recovery technologies, and attractive natural gas prices encouraged the industry to accelerate its development activity in other shale plays. The combination of two technologies- horizontal drilling and hydraulic fracturing- made it possible to produce shale gas economically, and from 2006 to 2010 U.S. shale gas production grew by an average of 48 percent per year (AOE 2011). The same game changing strategy of multiple transverse fractures created in a horizontal well that has worked so well for shale gas has also proven successful for shale oil.

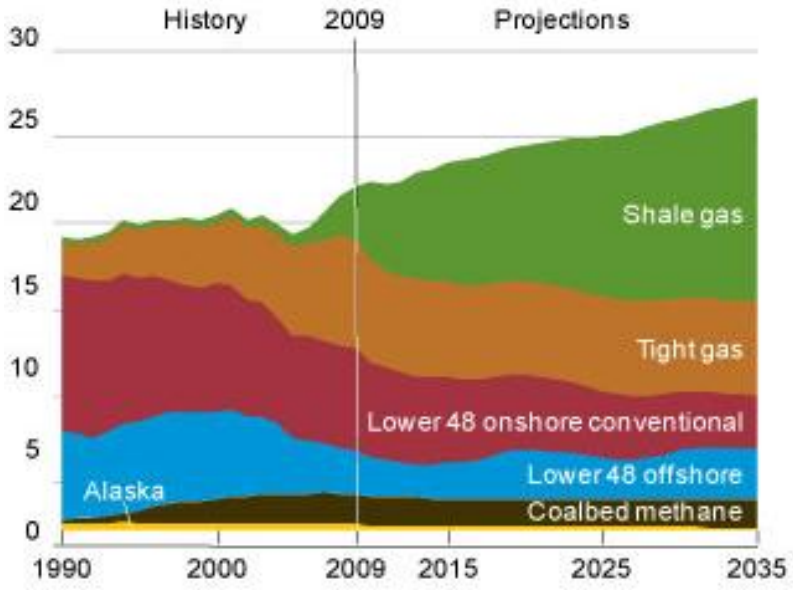

Figure 2: U.S. natural gas production in tcf/year, 1990-2035 (AEO 2011)

Figure 3, from AOE 2011, shows the U.S domestic crude oil production by source. The report reiterates that the growing shale oil resources coupled with rising world oil prices and technology advancement contributes to increased domestic crude oil production from 2009 to 2035. It states that the while the Bakken shale oil contributes to growth in the Rocky Mountain Region, the growth in the Gulf Coast region is spurred by the newly discovered Eagle Ford shale formation. Also, oil production from Avalon shale formation is offsetting the decline in oil production in the Southwest region.

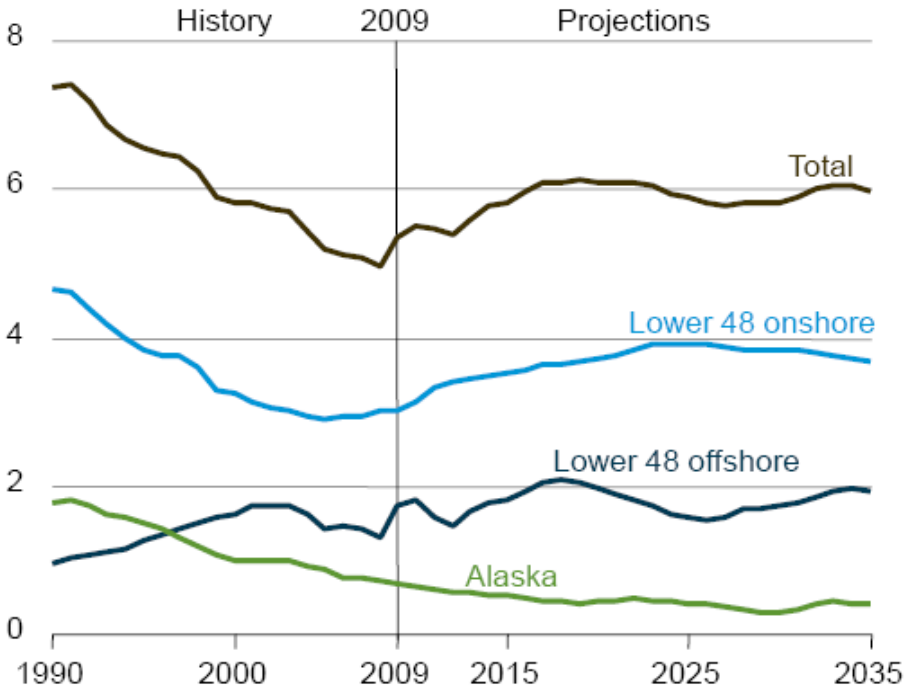

Figure 3: U.S. domestic crude oil production by source in MMBOPD, 1990-2035 (AEO 2011)

1.2 Oil shale and shale oil

All-too-often oil shale produced in Colorado is confused with shale oil plays like the Bakken shale, Eagle Ford shale and the Avalon shale mentioned above. There's a huge difference between oil shale and oil produced from shale reservoirs, called shale oil. Oil shale is rock that contains a solid organic compound known as kerogen. Oil shale is a misnomer because kerogen isn't crude oil, and the rock holding the kerogen often isn't even shale. To generate liquid oil synthetically from oil shale, the kerogen-rich rock is heated to as high as 950 degrees Fahrenheit (500 degrees Celsius) in the absence of oxygen, known as retorting. Oil shale remains a promising, yet expensive-to-produce resource that may eventually see more development.

Shale oil, unlike oil shale, does not have to be heated over a period of months to flow into a well. And the oil produced from these plays is premium crude; of better quality on average than West Texas Intermediate (WTI), the US standard crude that is the basis for NYMEX futures. Shale oil plays such as the Bakken, Eagle Ford and the Avalon shale have far more in common with unconventional gas plays such as Appalachia's Marcellus shale and Louisiana's Haynesville shale than they do with Colorado's oil shale. Shale oil is the crude oil that is produced from tight shale formations such as the Niobrara shale of Colorado, the Bakken shale of North Dakota, the Eagle Ford shale of Texas, and the Avalon shale of West Texas and South New Mexico. This study is about shale oil.

1.3 Production from unconventional shale oil and gas plays

While drilling a vertical well and perforating the pay interval leads to economic flow rates and economic volumes of oil and gas for conventional reservoirs, the same is not possible for unconventional reservoirs because of the low permeability of these reservoirs. To produce economic volumes from the unconventional reservoirs, a combination of increased oil and gas prices and improved technology of horizontal drilling and multi-stage fracturing are required.

After decades of a progression of well designs from a simple vertical well, to a vertical well with massive hydraulic fracture, to a horizontal well, finally horizontal well technology was adapted for shale gas reservoir development; by adding multiple transverse hydraulic fractures to provide significantly more contact with the reservoir, which is needed because shale permeability is very low. The combination of horizontal well with multistage transverse fractures (shown in **Figure 4**) has proven successful for shale gas reservoir development. Today the completions include many more fractures that are spaced closer together. This strategy is proving successful for shale oil as well.

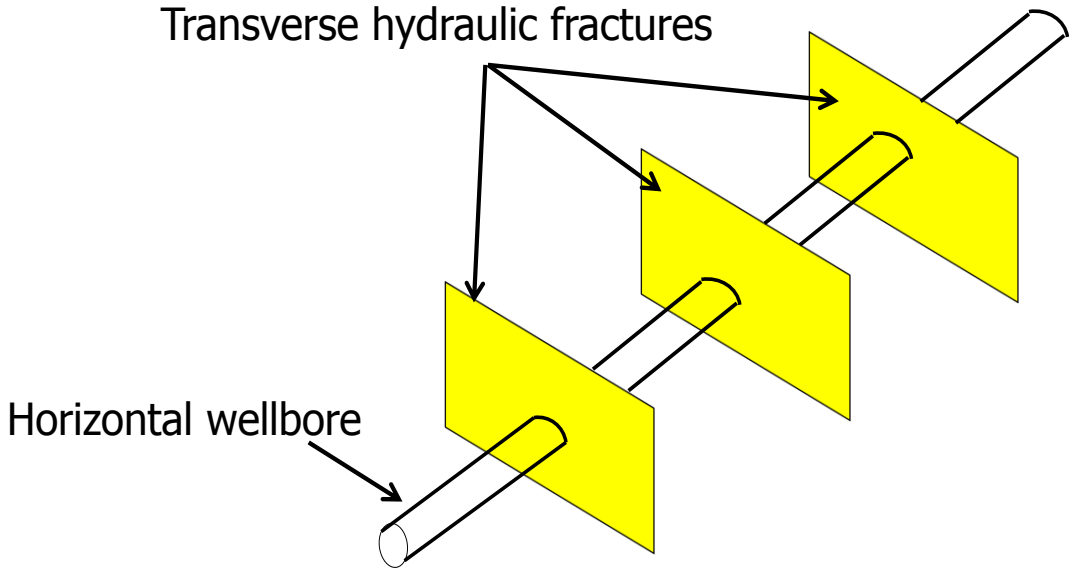

Figure 4: Illustration of multistage hydraulic fracture horizontal well (Song et al. 2011)

1.4 Objective of the current study

The objective of the current study is to evaluate the recovery potential for shale oil produced both above and below the bubble point pressure from very low permeability unconventional shale oil formations. As for conventional oil and gas, shale oil is limited to lower recovery efficiency than shale gas because oil has higher viscosity than gas and because two phase flow occurs in the formation below the bubble point. Also, often, because oil compressibility is much lower than for gas, the initial attractive production rates decline rapidly thus making shale oil wells economically marginal and sometimes operationally unattractive. In order to efficiently produce these reservoirs, it is important to understand fundamentally the different parameters of the effective stimulated rock volume (SRV): the rock, formation fluid and the created fracture properties. These significantly impact the long term production performance of these resources.

Chapter II indicates the known properties of the recently discovered Eagle Ford shale formation. Then Chapter III describes the simulation base case and the results the model provides. Chapter IV provides sensitivity studies investigating the role of the formation permeability, fracture spacing, fracture half-length, fracture conductivity, critical gas saturation, Corey oil and gas exponents, rock compressibility, flowing bottom-hole pressure, and reservoir permeability in the well economics and the ultimate recovery efficiency considering flow both above and below the bubble point pressure and using known properties of the Eagle Ford shale play. The sensitivity studies provide considerable insight about the long-term production behavior than can be expected in these types of wells. Chapter V explores the implications of the sensitivity study results

and contrasts shale oil production from shale gas and from conventional oil production. Finally, we summarize the main conclusions from this research.

CHAPTER II

EAGLE FORD SHALE PLAY

This chapter describes the geological setup, mineralogical constituents for the Eagle Fords shale formation that are important in designing and completing the typical well type in this formation and differentiate it from other earlier discovered shale formations such as the Barnett and the Haynesville shales. The chapter explains the areal extent of the Eagle Ford shale and its three different hydrocarbon containing areas: the gas window, the condensate window and the oil window. Actually, it is the oil rich area that has caught the eyes of the developers. Typical properties for the oil window in this shale will be used for the simulation and sensitivity studies in Chapter III and Chapter IV.

2.1 Hydrocarbon plays in the Eagle Ford shale

The Eagle Ford shale has long been known as a shale resource rock, but only recently has it been recognized as a viable shale play formation. **Figure 5** shows the Eagle Ford shale play, located in south Texas, extending over an area of almost 50 miles wide and 400 miles in length, and is in its infancy in terms of development compared to other shale plays in the USA. The Barnett shale has been commercially productive since the 1980s, the Haynesville since 2005 but the Eagle Ford has started producing only since 2009. The Eagle Ford formation has become a very active development in the North America because of the high volumes of liquid-rich hydrocarbons it is capable of producing. The types of hydrocarbons produced from the Eagle Ford shale vary from dry gas to gas/condensate to oil, making it a liquid-rich play. The direction of phase change from liquid to gas in the Eagle Ford shale is from north to south and from shallow to

deep, where oil is mainly present in the shallowest northern section. Figure 5 shows the oil (green), condensate (orange) and dry gas (red) producing windows.

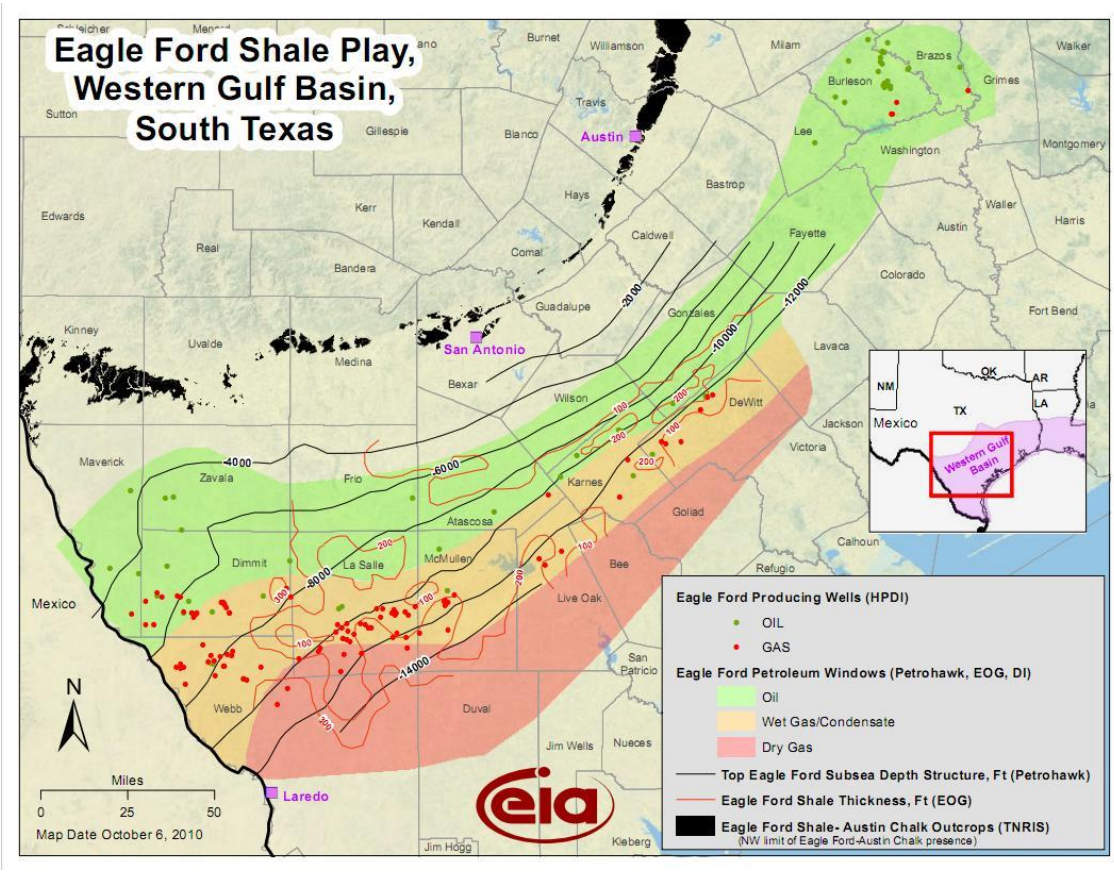

Figure 5: Eagle Ford shale play (Energy Information Administration, 2011)

2.2 Geology

Figure 6 (Condon and Dyman, 2006) shows how the stratigraphic column varies through the Eagle Ford across the play. The Eagle Ford shale lies above the Buda limestone and is overlain by the Austin Chalk. The late-cretaceous shale formation

covers a laterally extensive area from Maverick County in the west, all the way across the state to the eastern county of Burleson, and beyond (Figure 5).

Condon and Dyman (2006) described the geology, structural features, and depositional environment of the Eagle Ford, as well as the hydrocarbon-migration mechanism. Figure 5 illustrates how some basic structural features of this shale vary

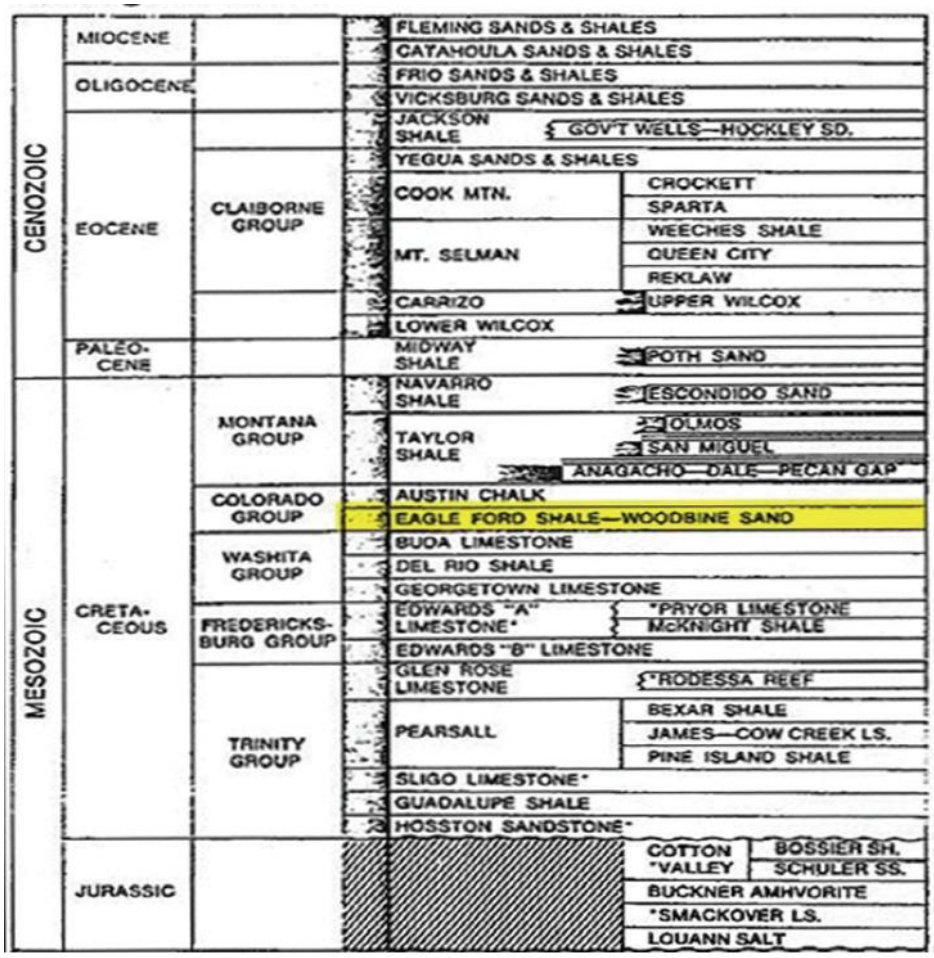

Figure 6: Stratigraphic column through south Texas (Condon and Dyman, 2006)

significantly across the play; for example, gross height varies from 100 to 300-ft thick, depth varies from 2,500 to 14,000 ft., pressure gradient varies from 0.55 to 0.85 psi/ft., and bottom-hole temperature varies from 150 ^{o}F to 350 ^{o}F. The formation produces dry gas at around 14,000 ft., condensate around 10,000 ft., and oil at around 8,000 ft. depth. It is interesting to note that in the same formation, the denser liquid hydrocarbons are found at shallower depth than the gas which is found at greater depth. Also, while the liquid hydrocarbons are somewhat over-pressured, the gas is at a much greater over-pressured. These observations reflect the very low permeability of the shale.

Although widely known as shale, the Eagle Ford formation is actually composed of organic-rich calcareous mudstones and chalks that were deposited during the two transgressive sequences, the upper and lower Eagle Ford. The lower Eagle Ford is organically richer and produces more hydrocarbons than the upper Eagle Ford. Bazan, L.W., et al. 2010 suggest that this is most likely due to a more oxygenated environment as depth decreases. The Austin Chalk has excellent reservoir characteristics, particularly where it has been fractured, and the hydrocarbons found within it were sourced by the Eagle Ford formation. The makeup of the Eagle Ford rock (calcareous mudstones and chalks) makes this play significantly different than other well-known unconventional plays such as the Barnett, Haynesville, and Marcellus shales, all of which are found in primarily siliceous environments.

2.3 Mineralogy

Figure 7 shows a ternary plot based on quartz, total clay, and total carbonate with the compositional fields outlined for the Eagle Ford shale play along with the

famous Barnett shale play. It shows that the Eagle Ford shale is mainly a clay-rich limestone with very low quartz content .The low quartz content makes it a less brittle (more ductile) with a low Young's Modulus (YM) of around $2 \cdot 10^6$ psi. In contrast, the Barnett shale is mainly quartz which makes it more brittle (less ductile) with a high YM of around $6 \cdot 10^6$ psi. **Figure 8** illustrates the Brinell hardness number (BHN) from core tests of various shale reservoirs in North America. It shows that the Eagle Ford shale is more similar to the "softer" Haynesville shale than to the hard Barnett shale.

Also, data from the whole-core testing on the Eagle Ford shale (Stegent et al. 2010) indicates that because the rock is relatively soft (low YM), it is prone to proppant embedment. **Figure 9** (Cipolla et al. 2008) illustrates that the embedment in the Barnett shale at the 5,000 psi closure stress will have 0.20 grain diameter of embedment, while the embedment in the Eagle Ford shale at 5,000 psi closure stress can have an 0.6 grain diameter of embedment.

The typical mineralogical properties of the Eagle Ford shale, along with the multi-phase flow expected in the production, makes its development different from the other shale plays.

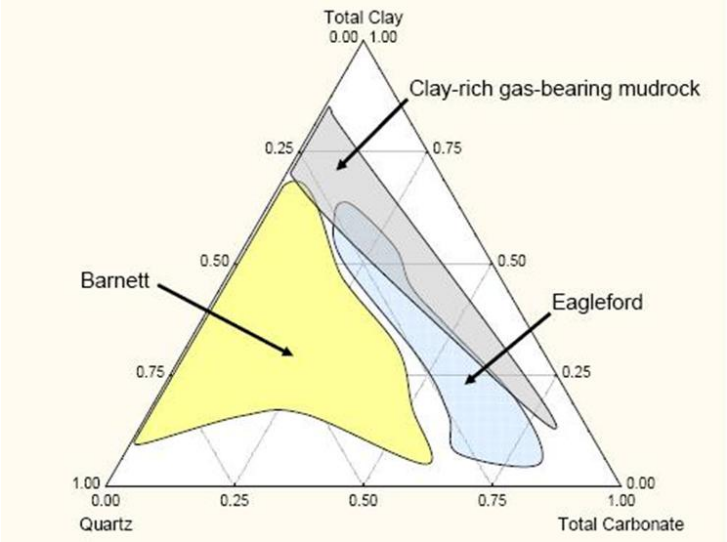

Figure 7: Mineral composition in Eagle Ford shale and Barnett shale (Passey et al. 2010)

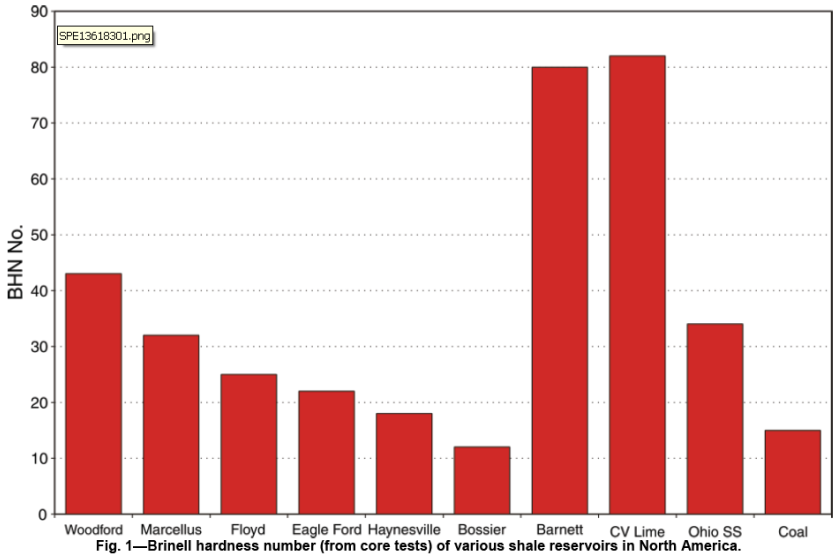

Figure 8: Brinell hardness number from core tests of various shale reservoirs in North America (Modified from Stegent et al. 2010)

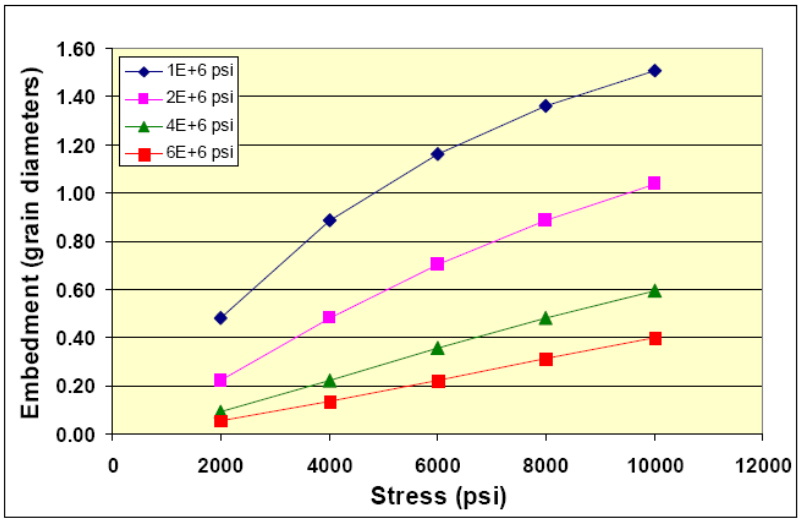

Figure 9: Proppant-embedment simulation for various YM vs. closure stress (Cipolla et al. 2008). The Eagle Ford shale has YM of ~2E6 psi while the Barnett shale has YM of ~7E6 psi

2.4 Stimulation treatment in the Eagle Ford shale play

Figure 10 (Mullen et al. 2010) shows the fluid system recommendation based on the brittleness determined for the shale. Rickman et al. (2008) explained the concept of rock brittleness which combines both Poisson's Ratio (rock ability to fail under stress) and Young's Modulus (maintain a fracture once the rock fractures). The brittleness of the Eagle Ford shale is markedly different than the Barnett shale.

The Barnett shale is a very hard, brittle formation (Brinell hardness number of 80) that contains many natural fractures, and has little, if any, horizontal stress anisotropy (the difference between the maximum and the minimum horizontal rock stress). This allows a complex network of fractures to be created rather easily by using a low-viscosity fracturing fluid. The high-YM rock tends to have little or no proppant embedment and it's easy to open the natural fractures during stimulation treatment as

there is very little difference between the maximum and the minimum stresses in the rock. Under these reservoir conditions, a slick water frac with low volumes of very small-mesh proppant has been relatively effective. The reservoir conditions of the Barnett shale lend themselves to being stimulated with slick water, which can provide sustainable production results (Stegent, N.A. 2010).

The Eagle Ford shale is significantly different. The Eagle Ford formation is a softer rock (BHN No. 22) and could potentially have more stress anisotropy, which allows a more planer-type fracture. The low YM indicates that the rock is relatively soft and prone to proppant embedment; therefore, low concentration of small-mesh proppant may not be as effective as in the Barnett formation. Higher concentration of larger-mesh proppant placed using hybrid fluid systems provide sufficient conductivity to overcome embedment and multiphase flow. **Figure 11** (Stegent, N.A. 2010) shows that cores of the Eagle Ford reservoir rock might not have a lot of visible natural fractures, but micro-fractures can be present. This means that a balance of net pressure may be required to maintain small fracture offsets along weak bedding planes and fissures during the stimulation treatment.

Brittleness	Fluid System	Fracture Geometry	Fracture Width Closure Profile	Proppant Concentration	Fluid Volume	Proppant Volume
70%	Slick Water			Low	High	Low
60%	Slick Water					
50%	Hybrid					
40%	Linear					
30%	Foam					
20%	X-Linked					
10%	X-Linked			High	Low	High

Figure 10: Fluid system recommendations based on the brittleness of shale formation (Mullen et al. 2010)

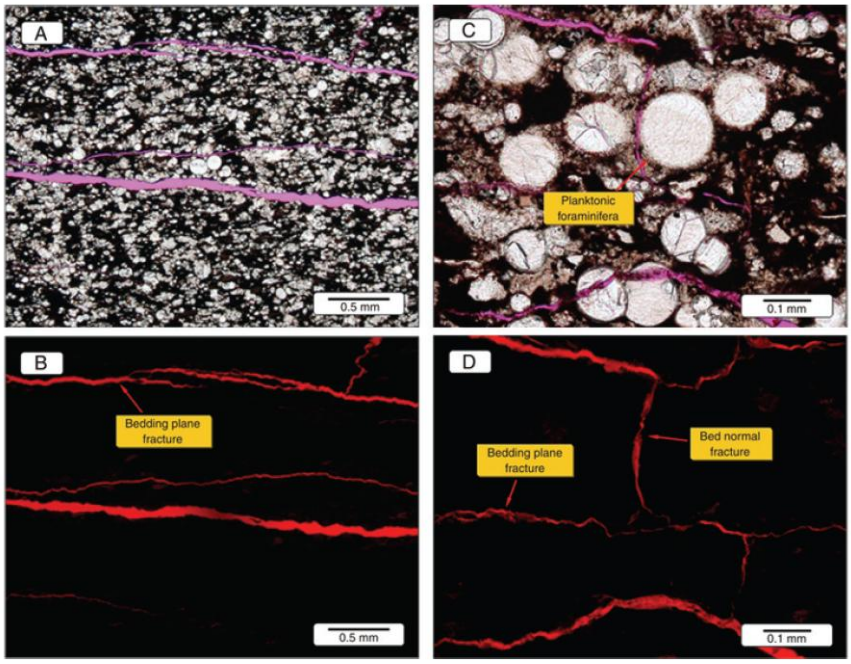

Figure 11: Normal and bedding-plane fractures from Eagle Ford cores (Stegent et al. 2010)

Hence, the typical completion type in the oil window of the Eagle Ford shale formation consists of using cross linked polymer as against slick water in other shale formations like Barnett shale. Also, because of low YM of the formation, the typical fracture geometry expected in this formation is a planer type fracture as against complex fractures in other relatively hard formations (high YM). Further, the proppant needed in this formation should be of high quality as the formation is soft (high proppant embedment) and proppant pack permeability is expected to degrade as after the onset of multi-phase flow will from the formation. **Figure 12** shows a single-fracture stage, with no-flow boundaries, which is modeled in the all the simulations in Chapter III and Chapter IV.

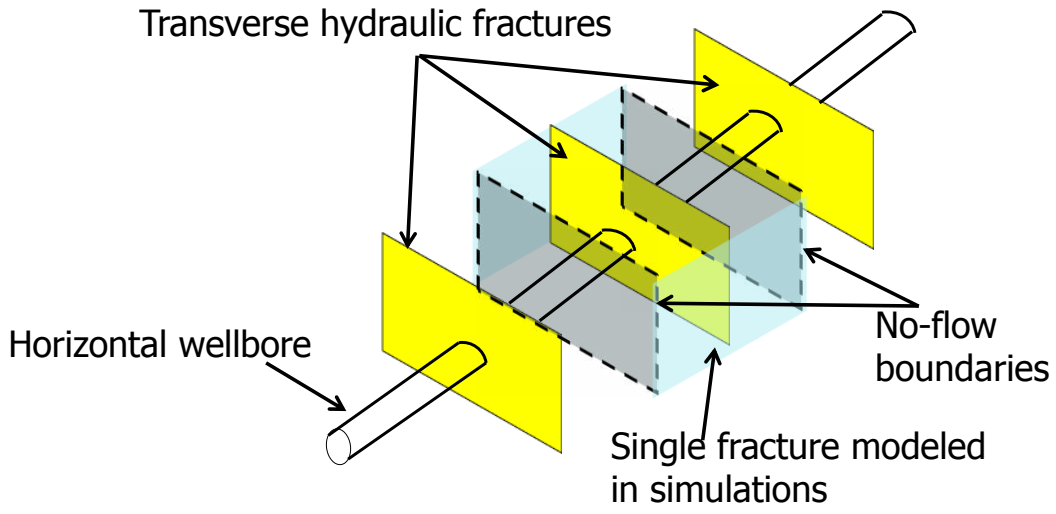

Figure 12: Illustration of single fracture stage (with no-flow boundaries) modeled in the simulations

CHAPTER III

BASE CASE RESERVOIR SIMULATION

Using rock, fluid and completion type parameters consistent with the description in Chapter II, this chapter describes the base case simulation model setup for the typical Eagle Ford shale well. We provide the model setup, input parameters, and describe base case simulation results. Then we compare modeled production of shale oil from this very low permeability reservoir to conventional reservoir flow behavior.

3.1 Introduction

Unconventional shale oil and gas reservoirs like Eagle Ford shale requires horizontal well drilling with multiple transverse hydraulic fractures, creating a stimulated reservoir volume (SRV). Within the SRV, oil and/or gas flow from the nano-darcy matrix shale to the created fracture network.

Rubin (2010) took forward the work of Mayerhofer et al. (2006) and Cipolla et al. (2010) and discussed the way forward for explicit modeling of a fracture network created in the stimulated reservoir volume (SRV). He first created an extremely fine grid reference solution (5-14 million cells in 2-D) which was capable of modeling fracture flow, using cells which are no longer than the width of actual fractures (assumed as 0.001 ft.), and flow into the fracture from the matrix using cells small enough to properly capture the very large pressure gradient involved. He showed that it is possible to accurately model flow from a fractured shale reservoir using logarithmically spaced, locally refined grids with fracture cells represented using approximately 2.0 ft. wide cells and maintaining the same conductivity as the original 0.001 ft wide fracture.

The present study uses the same technique of using logarithmically spaced, locally refined grids to model fracture flow, matrix to fracture flow and pressure and saturation changes for shale oil production from a stimulated reservoir volume.

3.2 Reservoir model

To investigate the effects of rock and fluid properties, fracture characteristics, and the completion parameters, we developed a homogenous 2-D reservoir well model of a horizontal well with multi-stage hydraulic fracture shown in. The dimensions and properties of this model are based on published information on the Eagle Ford Reservoir. In ultra-low permeability reservoirs, little fluid is produced outside the extent of the SRV. Hence, the simulation models the SRV dimensions, which are given by 2,000 ft long x 1,000 ft wide x 200 ft thick. We assume the well length consists of 10 transverse hydraulic fractures placed equally 200 ft. apart, with 500 ft. fracture half-length and the fracture height is 200 ft. Since we assume the fractures are identical, we model a single fracture (**Figure 13**) only. To get the oil rate/cumulative oil production for the entire well, the simulation results can be multiplied to the number of fracture stages. The results in all the graphics in this thesis are reported for only one single fracture.

Figure 13 shows the single fracture, with logarithmically spaced locally refined grids, used in all the simulation studies. Based on the description for Eagle Ford shale in Chapter II, the simulation model has a single porosity system.

As shown by work of Rubin (2010), it is not feasible for efficiently running the simulation with the use of 0.001 ft fracture width. Hence, the fracture cells are scaled to a 2.0 ft width so that they are more of a fracture conduit. The cells of the 2.0 ft wide

conduit are given the same fracture conductivity as the 0.001 ft wide cells. Assuming the fracture has 41.65 md permeability in a 2.0 ft width gives the same fracture conductivity of 83.3 md-ft as a 83,300 md fracture permeability in a 0.001 ft width. For the base case permeability of 0.0001 md (100 nano-darcy) and 500 ft fracture half length, the dimensionless fracture conductivity is 16,400, which is effectively infinite conductivity.

After trying several LGR grid sizes, we found that a 49x49x1 refinement of the grid cell having perforation, and 49x11x1 for all other cells in each of the 200 ft x 200 ft x 200 ft network fracture blocks in the SRV gave sufficient accuracy and that a smaller refinement did not appreciably change the result. The resulting locally refined grid is logarithmically spaced (to capture the large pressure drop and saturation changes near the matrix-fracture interface).

There are 4,562 grid cells in total in the base case model. Again, we are only modeling one fracture of the 10 fractures spaced every 200 ft and orthogonal to the well. The entire reservoir is initialized to 6,425 psi and the well produces for 30 years at a minimum pressure constraint of 1,000 psi and is initially subject to a maximum rate constraint of 1,000 STB/d.

Reservoir properties, hydraulic fracture properties, PVT properties and relative permeability end points for matrix and shale for this Eagle Ford shale oil model are presented in **Table 1**, **Table 2**, **Table 3**, and **Table 4**. The saturation is initialized to uniform oil with connate (irreducible) water value shown in Table 4.

Table 1: Reservoir properties for Eagle Ford oil window well setup

Initial Reservoir Pressure	6,425 psi
Porosity in Shale	0.06
Initial Water Saturation	0.3
Compressibility of Shale	$5 \cdot 10^{-6}$ psi^{-1}
Permeability of Shale	0.0001 md
Reservoir Thickness	200 ft.

Table 2: Hydraulic fracture properties for Eagle Ford oil window well setup

Fracture Stages	10
Fracture Spacing	200 ft.
Fracture conductivity	83.3 md-ft.
Fracture Half-length	500 ft.
Fracture Cell width	2 ft.

Table 3: PVT properties of oil used for Eagle Ford oil window well setup

Reservoir Temperature	255 ^{o}F
Bubble Point for Oil	2,398 psi
Solution Gas Oil Ratio	650 scf/stb
^{o}API for Oil	42
Under-saturated Oil Compressibility	$1 \cdot 10^{-5}$ psi^{-1}
Gas Specific Gravity	0.8

Table 4: Relative permeability end points for fracture and matrix

	Matrix	Fracture
N_o	5	1.5
N_g	2	1
S_{wi}	0.3	0.05
S_{org}	0.3	0.1
S_{gc}	0.05	0.0
k_{rg} at S_{org}	1	1

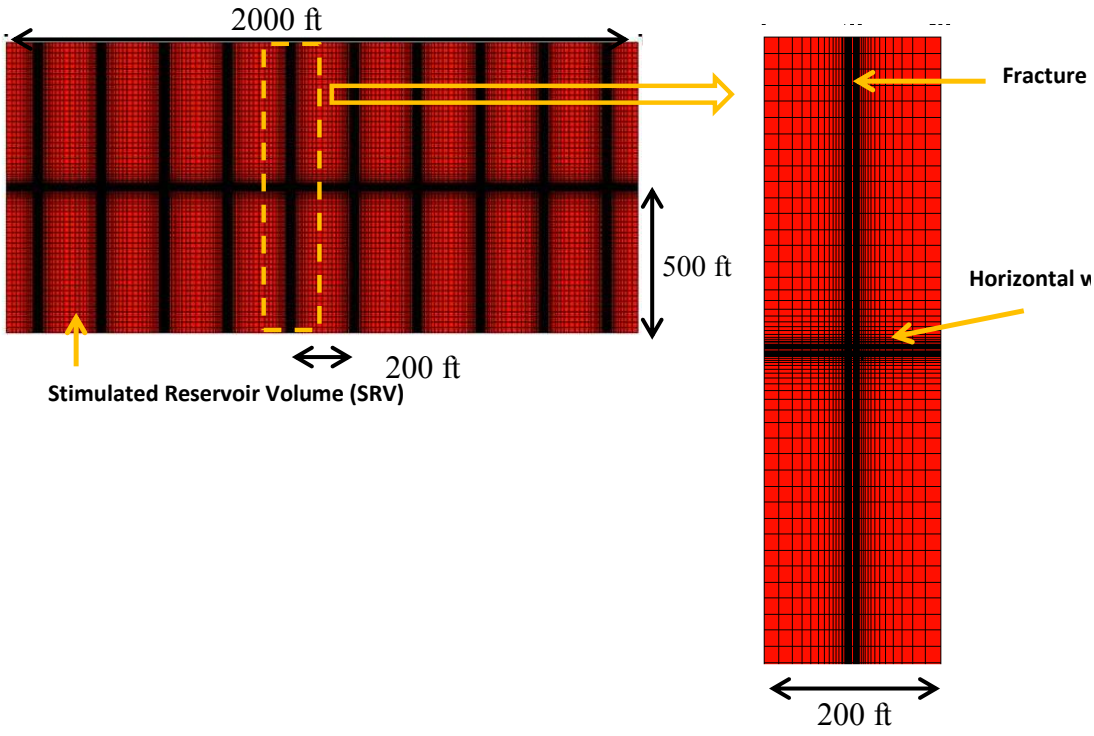

Figure 13: Illustration of single fracture, with logarithmically spaced locally refined grids, modeled for all the simulations. The oil rate/cumulative oil production results for the entire well can be obtained by multiplying the simulation results with the number of fractures in the SRV

3.3 Simulation results

Figure 14 shows the pressure variation, over a period of 30 years while the well is on production, in and around the hydraulic fracture, and **Figure 15** shows the gas saturation buildup for the same time periods. Note that the images for each time shown in Figure 14 and Figure 15 only represent half of the fracture shown in Figure 13. As noted before, the logarithmic gridding with local grid refinement enables accurate representation of steep pressure and saturation changes immediately near the fractures.

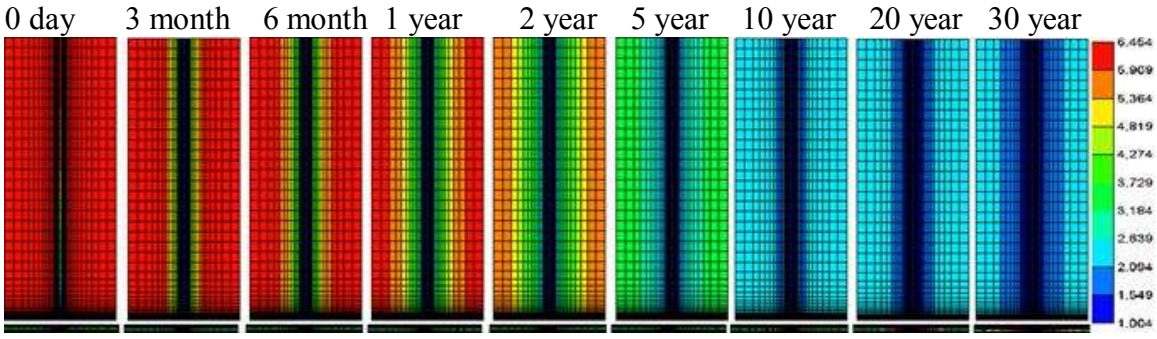

Figure 14: Pressure (psi) in the modeled fracture as a function of time

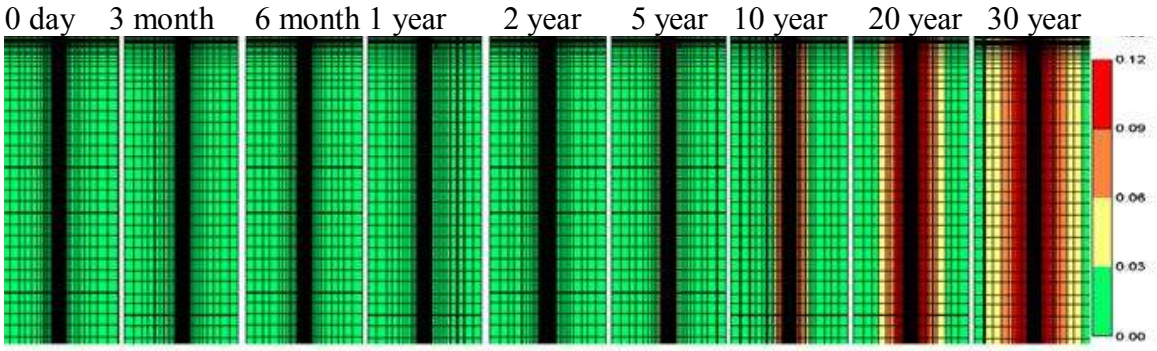

Figure 15: Gas saturation (fraction) in the modeled fracture as a function of time

Figure 16 a, b, c and **d** shows the base case simulation results for oil rate and cumulative oil production, log-log oil rate, average reservoir pressure and instantaneous gas oil ratio (GOR) versus time. All the simulation results are for production from a single fracture. The single fracture oil rate decreases from the initial rate of 200 STB/d to around 30 STB/d after 30 days of production and to 10 STB/d within 1 year (5% of Initial production rate). The oil production rate from a single fracture at the end of 30 years is 0.6 STB/d. The cumulative oil recovery from a single fracture at the end of 30 years is 27,000 barrels. This corresponds to a recovery factor of 11.64%.

The Ahmadi et al. (2010) model showed that production from shale reservoirs behave as they are controlled by transient linear flow. He showed that the behavior is characterized by half-slope on the log-log plot of gas rate vs. time. Figure 16 b shows a log-log plot of oil rate vs. time. Although the graph shows half-slope for almost 4 years (1,500 days), the slope is distorted by multi-phase flow (gas and oil) as the area immediately near the fracture goes below the bubble point.

The average reservoir pressure in Figure 16 decreases fast as the recovery in this reservoir is mainly by depletion drive and some solution gas drive. The reservoir pressure decreases from an initial pressure of 6,425 psi to 5,000 psi at the end of 1 year, to about 4,000 psi at the end of 2 years, to about 3,000 psi at the end of 5 years and after that the pressure stays fairly constant at about 2,000 psi till the end of 30 years as there is not much production from the reservoir.

The GOR stays fairly constant and close to the solution gas oil ratio of 650 scf/stb for the first two years (800 days). The GOR starts to increase slowly after that

and the GOR value is around 1,000 scf/stb at the end of 5 years (2,000 days). The GOR rises slowly after that and at the end of 30 years the final GOR is around 1,800 scf/stb. This slow rise of GOR with time is because of the steep pressure gradient near the well so that only a small area around the hydraulic fracture is in two-phase flow below the bubble point pressure. **Figure 17** shows the same base case results as in Figure 16 but with time axis on logarithmic scale.

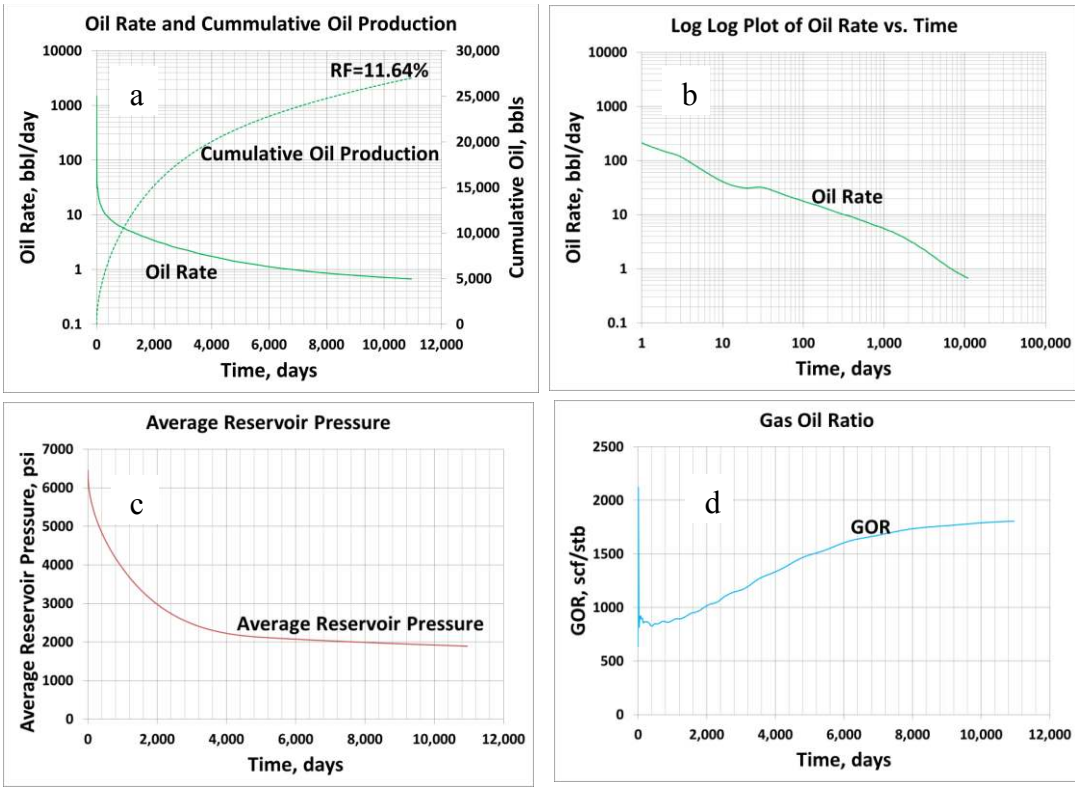

Figure 16: Base case simulation results for a single fracture only with a) oil rate and cumulative oil production, b) log-log plot of oil rate vs. time, c) average reservoir pressure, and d) instantaneous gas-oil ratio

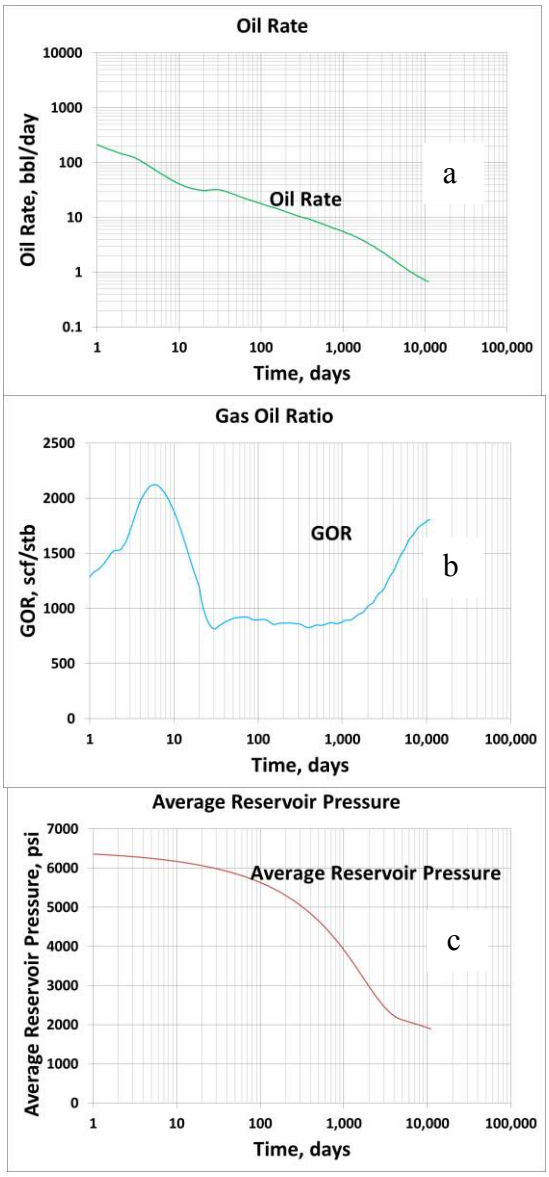

Figure 17: Base case simulation results – time axis on logarithmic scale

3.4 Conventional reservoir vs. unconventional reservoir production

It is instructive to compare the modeled production of shale oil from this very low permeability shale to conventional reservoir flow behavior. For the conventional reservoir case, the model setup is kept the same. Only the reservoir permeability is increased from the shale permeability of 0.0001 md to a typical conventional oil reservoir permeability of 100 md.

Figure 18 contrasts the results of the production from the unconventional nano Darcy permeability to a case of a conventional reservoir of 100 md permeability. The most important comparison is that while shale oil reservoir takes 30 years to produce about 12% of the original oil in place, the conventional reservoir of 100 md permeability with the same flowing bottom-hole pressure constraint of 1,000 psi produces 19% of the oil in only in year. The lower recovery factor for the unconventional reservoir is explained from the average reservoir pressure graph. Though recovery in both cases is by solution gas drive, while the average pressure can be reduced to the flowing bottom-hole pressure limit of 1,000 psi for the conventional reservoir case, it can only by reduced to 2,000 psi in case of unconventional reservoir because of lower permeability. To increase the 30 year recovery factor, the fractures should be spaced closer together.

The GOR for the conventional reservoir and unconventional shale oil also show marked difference. While the GOR for the conventional reservoir case rises steeply from an in initial solution GOR of 650 scf/stb to as high 20,000 scf/stb after one year of production, the lower permeability shale oil GOR rises only slowly and even at the end of 30 years of production the GOR is only about 2,000 scf/stb.

The results from the base case simulation model setup in this chapter will be used as reference for the different sensitivity studies done in Chapter IV.

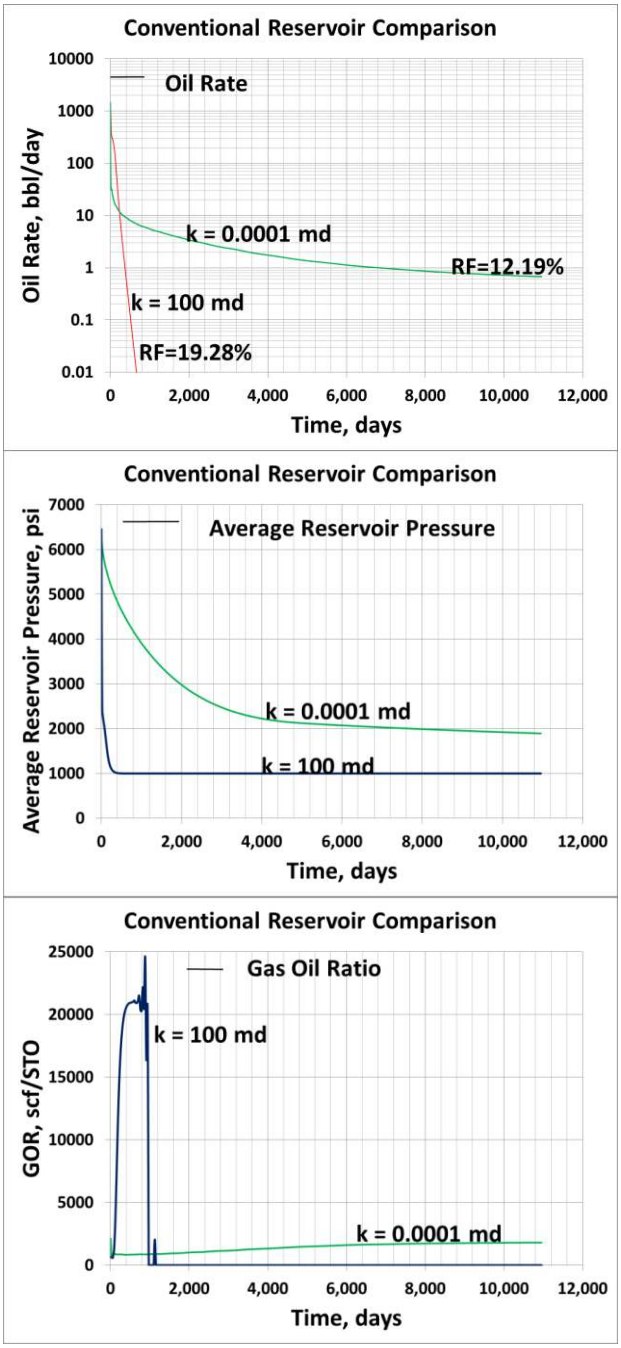

Figure 18: Conventional vs. unconventional reservoir production

CHAPTER IV

SENSITIVITY STUDIES ON PARAMETERS AFFECTING PRODUCTION PERFORMANCE FROM SRV

The production behavior and recovery of oil from the low permeability shale formation is a function of the rock, fluid and the fracturing operations. Sensitivity studies in this chapter illustrate the important parameters affecting shale oil production performance from the stimulated reservoir volume.

The parameters studied/discussed in this chapter include fracture spacing, fracture half-length, rock compressibility, critical gas saturation, flowing bottom-hole pressure, hydraulic fracture conductivity, and matrix permeability.

The results from the sensitivity studies can be used in not only designing better wells but also understanding the fundamental behavior of the shale oil production system.

4.1 Fracture spacing

A key question that needs to be answered while completing a well in the Eagle Ford formation is the fracture spacing. A completion engineer often struggles to find the optimum spacing and often requests a reservoir simulation engineer to generate the possible scenarios using computer models.

Figure 19 shows the results of the fracture spacing on the cumulative oil production, recovery factor, average reservoir pressure and instantaneous gas oil ratio. The fracture spacing used in the base case simulation is 200 ft. We selected three another fracture spacing scenarios of 50 ft, 100 ft, and 300 ft.

Though closer fracture spacing means more fracture stages and increased completion cost per well, it leads to not only higher cumulative oil production but also higher initial production rate and a higher ultimate recovery factor for the oil which means better drainage of the SRV. Net present value analysis can be used to determine optimum fracture spacing. Song, et al (2011) addressed this approach for shale gas well design.

The graph of average reservoir pressure for different fracture spacing shows that, the reservoir pressure can be lowered to a lower value in case of closer fracture spacing. The average reservoir pressure at the end of 30 years for 100 ft. spacing is close to the bottom hole pressure limit of 1,000 psi. For all higher values of fracture spacing, the reservoir pressure stays higher, leading to lower ultimate recovery.

The instantaneous gas oil ratio (GOR) graph mimics the average reservoir pressure behavior. For closer fracture spacing the GOR keeps rising higher as the reservoir can be drained to lower pressure as more of the reservoir is saturated and hence higher GOR.

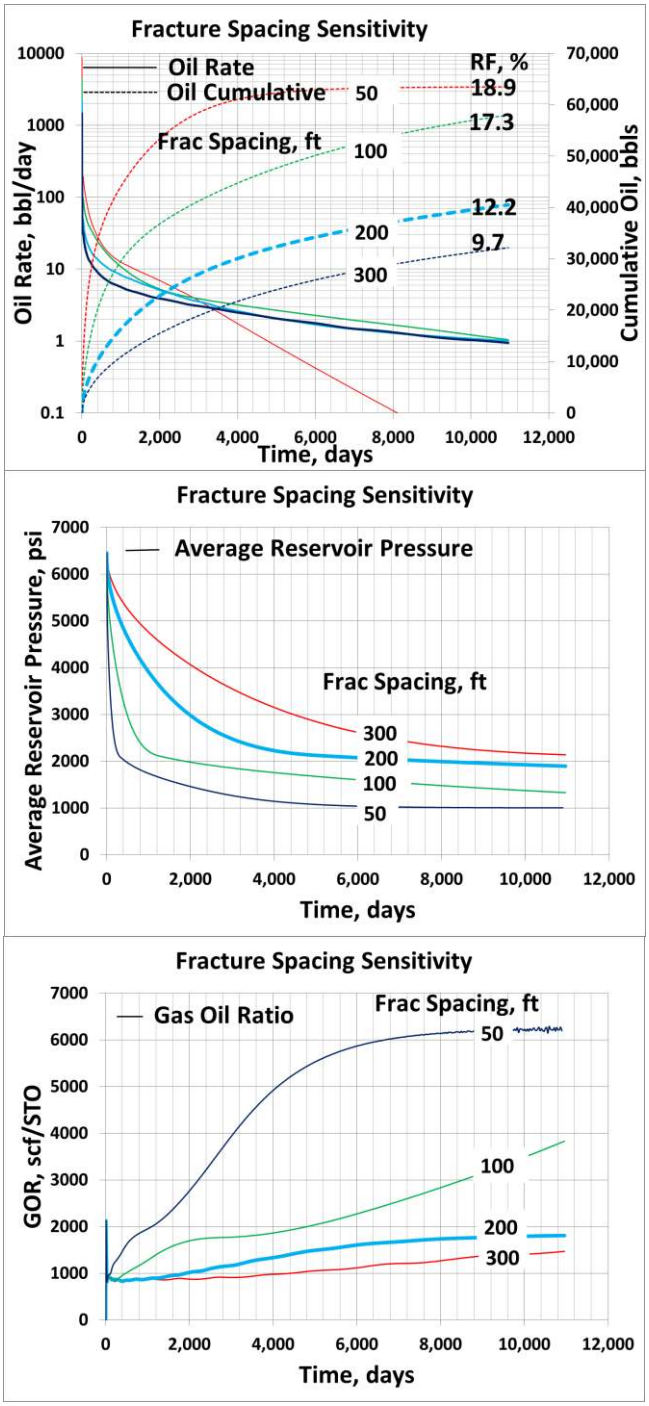

Figure 19: Fracture spacing sensitivity. Base case has fracture spacing of 200 ft, fracture half-length of 500 ft, rock compressibility of $5 \cdot 10^{-6}$ psi^{-1}, critical gas saturation of 0.05, flowing bottom-hole pressure of 1000 psi, fracture conductivity of 83.3 md-ft and matrix permeability of $1 \cdot 10^{-4}$ md

4.2 Fracture half-length sensitivity

Chapter II discussed the low YM of the Eagle Ford formation. As indicated, the typical fracture geometry expected in this formation is a planer type fracture as compared to complex fractures in other relatively hard formations (high YM) like the Barnett shale.

Figure 20 shows the results of the different fracture half-length on the cumulative oil production, recovery factor, average reservoir pressure and instantaneous gas oil ratio. The fracture half-length used in the base case simulation is 500 ft. We selected three another fracture half-lengths of 375 ft, 250 ft, and 125 ft.

The results show that large fracture half-length leads to higher cumulative oil production. The cumulative oil production increases in direct proportion to the fracture-half length. Although the recovery factor stays the same for all the scenarios at 12.2 %, the advantage is in that the one well can drain much higher volume of the reservoir and hence there is need for lesser number of wells in total. The average reservoir pressure and the instantaneous GOR stay the same for all the cases.

The completions job should be designed in such a manner so as to increase the fracture half-length so as to drain more fluid from each well.

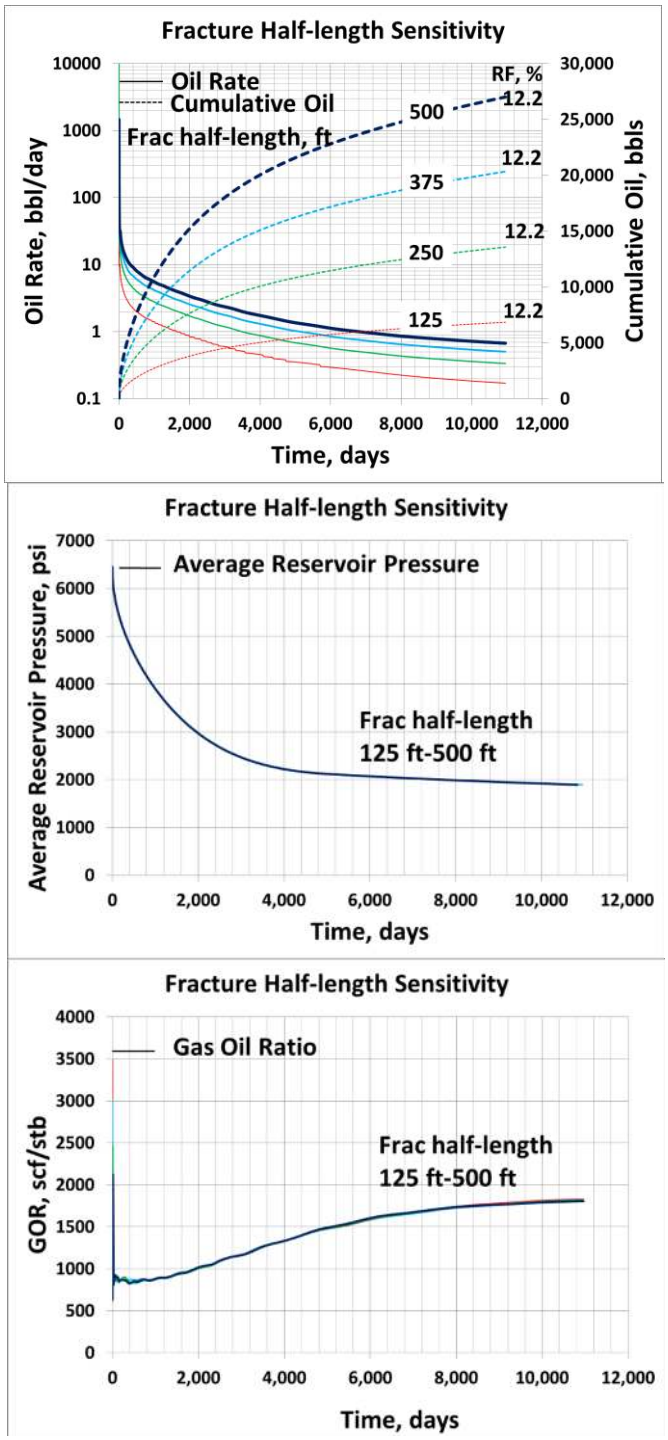

Figure 20: Fracture half-length sensitivity. Base case has fracture spacing of 200 ft, fracture half-length of 500 ft, rock compressibility of $5 \cdot 10^{-6}$ psi^{-1}, critical gas saturation of 0.05, flowing bottom-hole pressure of 1000 psi, fracture conductivity of 83.3 md-ft and matrix permeability of $1 \cdot 10^{-4}$ md

4.3 Rock compressibility sensitivity

Hall's (Hall, 1953) provided the general rock compressibility curves for sandstone and limestone reservoirs. Shale rock compressibility values and particularly for the Eagle Ford shale are not published in the literature.

Hsu and Nelson (2002) in their work commented that they expected the compressibility of the Eagle Ford shale to be on higher side because of the high amount of smectite (50%) in the clay minerals (38-88%).

Figure 21 shows the results of the for different rock compressibility values on the cumulative oil production, recovery factor, average reservoir pressure and instantaneous gas oil ratio. The rock compressibility value used in the base case simulation is $5 \cdot 10^{-6}$ psi^{-1}. We further selected three higher compressibility values of $15 \cdot 10^{-6}$ psi^{-1}, $25 \cdot 10^{-6}$ psi^{-1}, and $50 \cdot 10^{-6}$ psi^{-1}.

The results show that the cumulative oil recovery and the recovery factor can be much higher than it is for the base case if the Eagle Ford shale is found to be more compressible than it is assumed in our study in the base case. We suggest conducting lab studies for accurate determination of the rock compressibility values.

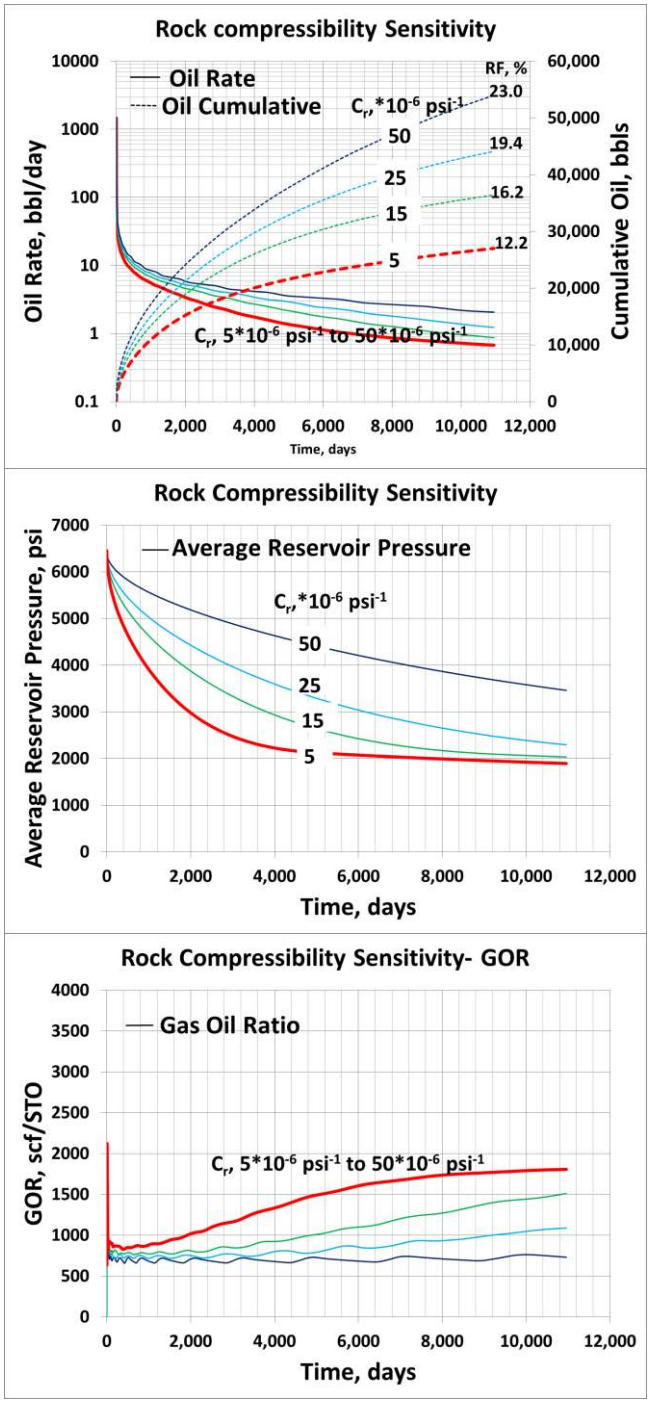

Figure 21: Rock compressibility sensitivity. Base case has fracture spacing of 200 ft, fracture half-length of 500 ft, rock compressibility of $5 \cdot 10^{-6}$ psi^{-1}, critical gas saturation of 0.05, flowing bottom-hole pressure of 1000 psi, fracture conductivity of 83.3 md-ft and matrix permeability of $1 \cdot 10^{-4}$ md

4.4 Critical gas saturation sensitivity

The critical gas saturation, S_{gc}, denotes the minimum gas saturation at which the gas molecules form a continuous phase and start moving during depressurization of an under-saturated liquid in a porous medium.

Figure 22 shows the results for different critical gas saturation values on the cumulative oil production, recovery factor, average reservoir pressure and instantaneous gas oil ratio. The S_{gc} value used in the base case simulation is 5%. We selected another three S_{gc} values of 2%, 10%, and 20%.

The figure for the cumulative oil shows that the recovery factor varies from a low of 11% to a high of 17.6% for a critical gas saturation of 2% and 20% respectively. The higher recovery in case of high gas saturation is due to the gas staying in the pore spaces and pushing the oil out of the pore spaces before it finally starts moving at the critical gas saturation value.

The GOR curve also explains the higher recovery for higher critical gas saturation. The GOR stays low for higher critical gas saturation as the gas stays inside the pore space instead of flowing to the well.

The results underscore the importance of understanding the two-phase flow in shale. The results could change the well drilling and completion strategies which are still in nascent stage and require a lot of capital cost for drilling each well in the shales. The critical gas saturation is a critical parameter and justifies core analysis studies.

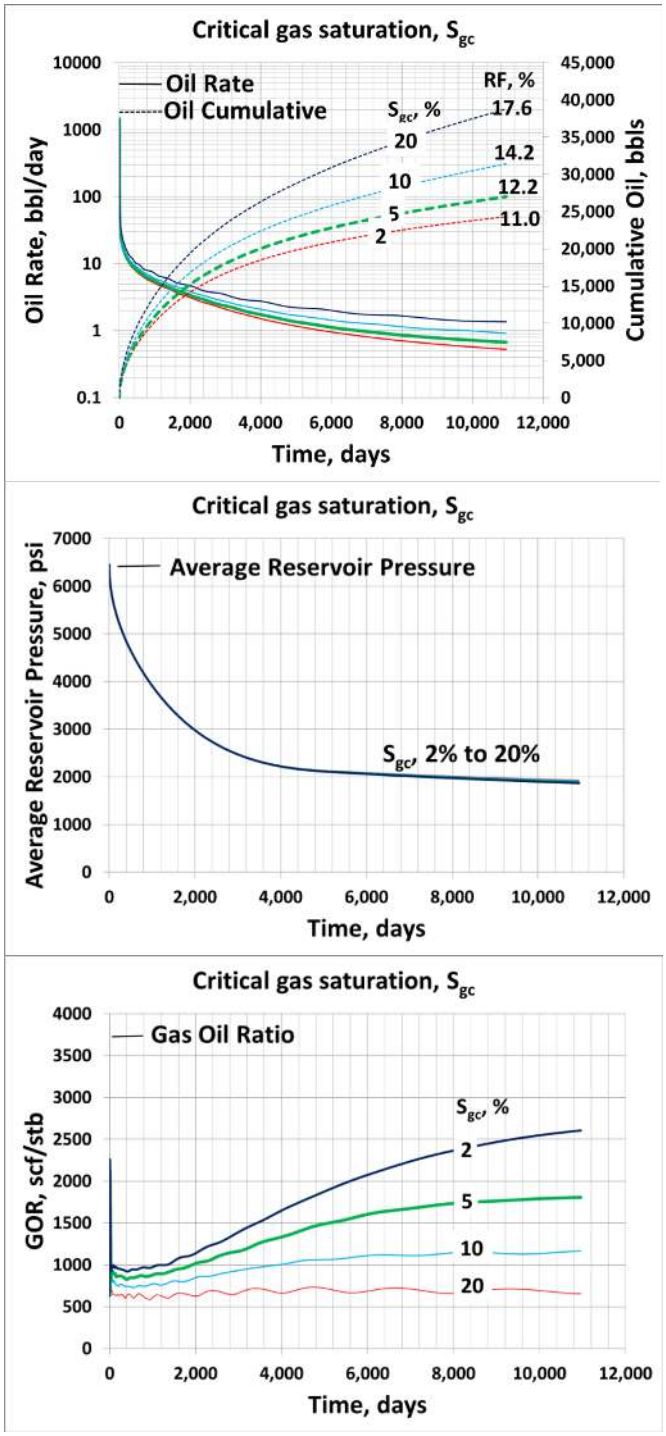

Figure 22: Critical gas saturation sensitivity. Base case has fracture spacing of 200 ft, fracture half-length of 500 ft, rock compressibility of $5 \cdot 10^{-6}$ psi^{-1}, critical gas saturation of 0.05, flowing bottom-hole pressure of 1000 psi, fracture conductivity of 83.3 md-ft and matrix permeability of $1 \cdot 10^{-4}$ md

4.5 Flowing bottom-hole pressure (FBHP) sensitivity

The Eagle Ford reservoir is over-pressured (0.55-0.85 psi/ft pressure gradient). Most of wells start on production to the surface without artificial lift. But the well soon needs to be put on artificial lift as the shale pressure declines and the head of the liquid in the production tubing becomes greater than the reservoir pressure.

Since the recovery in the Eagle Ford reservoir is expected to be primarily by depletion only, a lower flowing bottom-hole pressure (FBHP) aids in extra recovery from the reservoir.

Figure 23 shows the results for different flowing bottom-hole pressure values on the cumulative oil production, recovery factor, average reservoir pressure and instantaneous gas oil ratio. The FBHP value used in the base case simulation is 1,000 psi. The bubble point for the oil is 2,496 psi. We selected one FBHP value of 2,500 psi (under-saturated case) and other two FBHP values of 1,500 psi, and 500 psi (saturated-case).

The recovery factor for the oil produced above the bubble-point (under-saturated case) is only 7.23%. The same is boosted to 11.64%, 12.19%, and 12.43% for flowing bottom-hole pressure of 1,500 psi, 1000 psi and 500 psi (saturated-cases).

The GOR mimics the average reservoir pressure behavior. The lower the FBHP, the more the instantaneous gas oil ratio. As expected, we found that the lower the FBHP, the greater the recovery that would be from this shale oil reservoir.

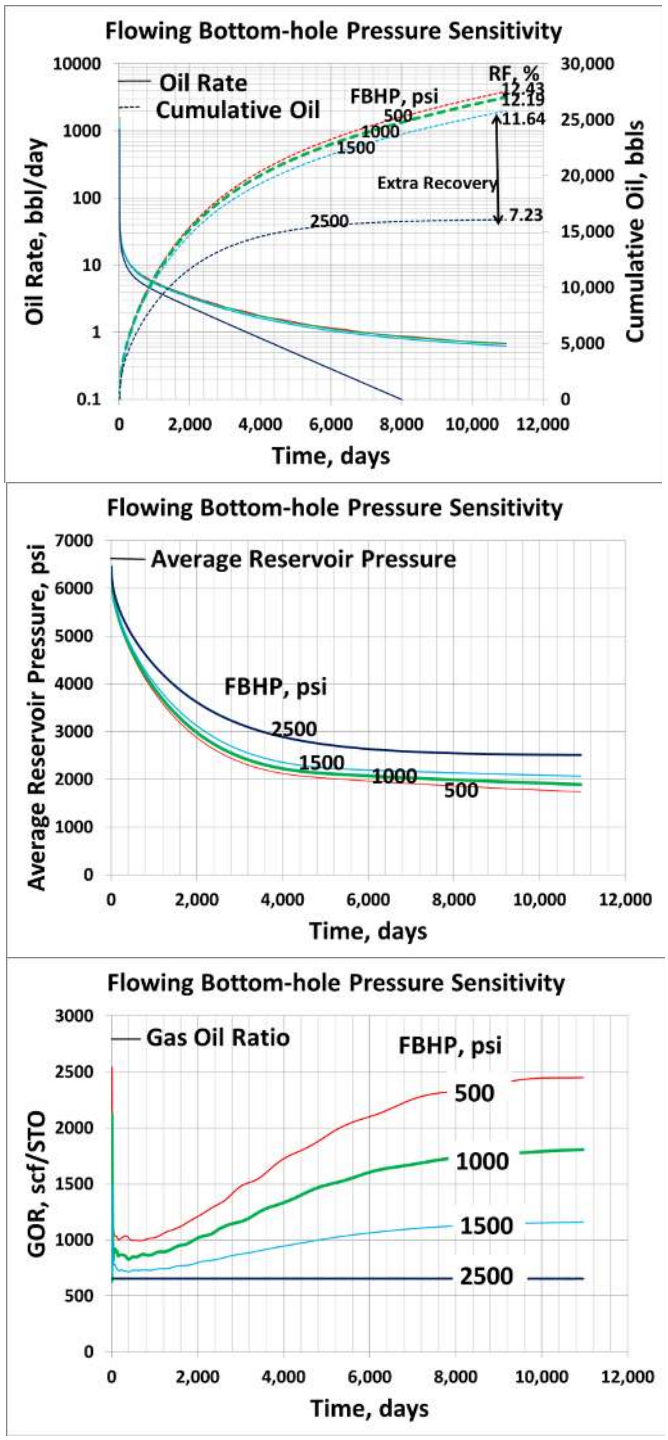

Figure 23: Flowing bottom-hole pressure sensitivity. Base case has fracture spacing of 200 ft, fracture half-length of 500 ft, rock compressibility of $5 \cdot 10^{-6}$ psi^{-1}, critical gas saturation of 0.05, flowing bottom-hole pressure of 1000 psi, fracture conductivity of 83.3 md-ft and matrix permeability of $1 \cdot 10^{-4}$ md

4.6 Fracture conductivity sensitivity

The problem of proppant embedment and expected multi-phase flow in the created hydraulic fractures can lead to actual values of fracture conductivity (k_fW, md-ft) and the dimensionless conductivity, C_{fD} values in the created fractures order of magnitude lower than the values reported in the laboratory.

The dimensionless conductivity, C_{fD}, is defined as,

$C_{fD} = k_fW/ kx_f$

For the base case;

$C_{fD} = 10{,}000$ md x 0.00833 ft/0.0001 md x 500 ft

$C_{fD} = 1{,}666$

For $C_{fD} > 25$, the fracture is considered of infinite conductivity (effectively no pressure drop in the fracture); otherwise it is considered finite conductivity.

Figure 24 shows the results for different C_{fD} values for the created hydraulic fractures on the cumulative oil production, recovery factor, average reservoir pressure and instantaneous gas oil ratio. As shown in the calculations above, the C_{fD} value used in the base case simulation is 1,666 which make its fracture of infinite conductivity. We selected C_{fD} values of 16,683 and 16.6. For the C_{fD} value of 16.6, the fracture becomes finite conductivity.

The results of the cumulative oil production show that when the C_{fD} value is greater than 25, i.e. infinite conductivity fracture; oil recovery is not affected by the absolute values of fracture conductivity. On the other hand the oil recovery drops suddenly as C_{fD} value becomes less than 25 i.e. finite conductivity fracture.

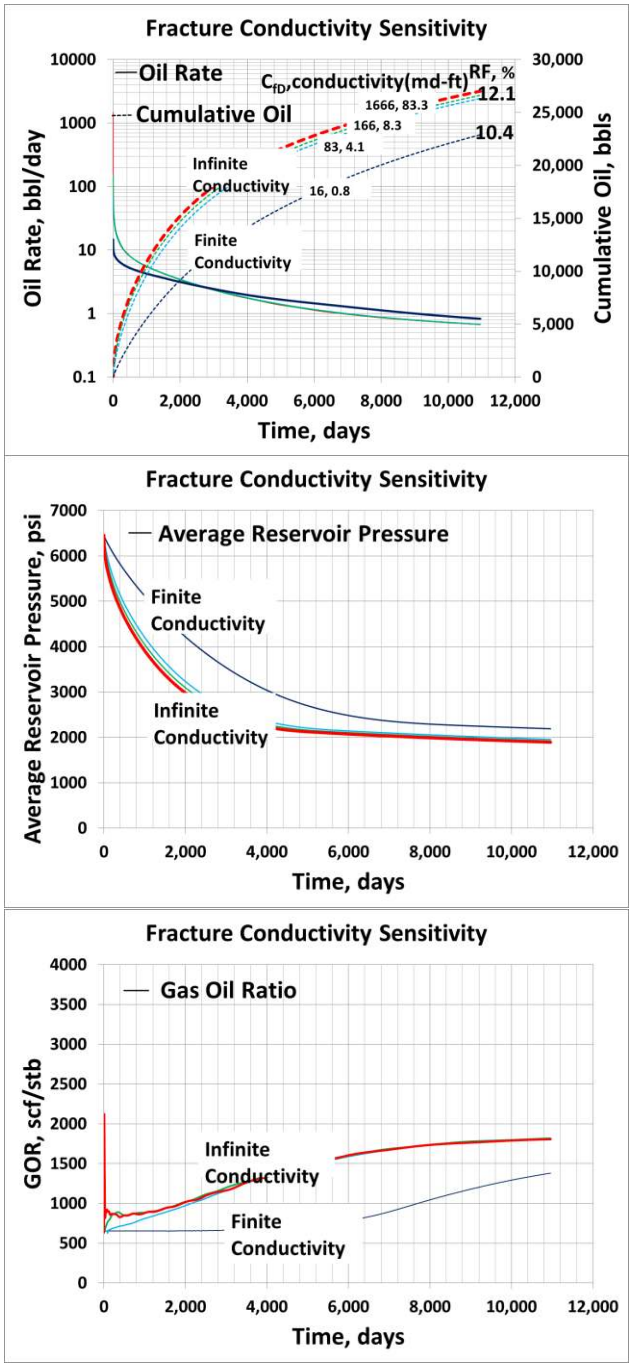

Figure 24: Fracture conductivity sensitivity. Base case has fracture spacing of 200 ft, fracture half-length of 500 ft, rock compressibility of $5 \cdot 10^{-6}$ psi^{-1}, critical gas saturation of 0.05, flowing bottom-hole pressure of 1000 psi, fracture conductivity of 83.3 md-ft and matrix permeability of $1 \cdot 10^{-4}$ md

The reservoir pressure declines to the same values for all the effectively infinite conductivity cases. For finite conductivity, the reservoir pressure cannot be reduced as in the case of infinite conductivity case and hence leads to a lower recovery. The GOR shows the slow increasing trend in general. Though for finite conductivity case, the GOR rises much slower than for the effectively infinite conductivity case as the decline in reservoir pressure is much slower.

The study shows that oil production is not affected by the absolute values of the fracture permeability while the C_{fD} value remains greater than 25 i.e. for effectively infinite conductivity fractures. On the other hand, cumulative oil production drops sharply as soon as the fracture C_{fD} value becomes less than 25 i.e. for finite conductivity fracture. Hence it's very important to make sure the proppant used is of high quality to retain its permeability.

4.7 Matrix permeability sensitivity

Measurement of accurate permeability, k, in the shale formations like Eagle Fords shale is a big challenge. The conventional ways of determining reservoir permeability like pressure transient testing or formation testing usually do not work in these reservoirs due to very slow response of the formation.

Figure 25 shows the results for different matrix permeability, k, values on the cumulative oil production, recovery factor, average reservoir pressure, and instantaneous gas oil ratio. The k value used in the base case simulation is $1 \cdot 10^{-4}$ md (100 nano-darcy). We selected another three k values of $1 \cdot 10^{-3}$ md, $5 \cdot 10^{-4}$ md and $5 \cdot 10^{-5}$ md.

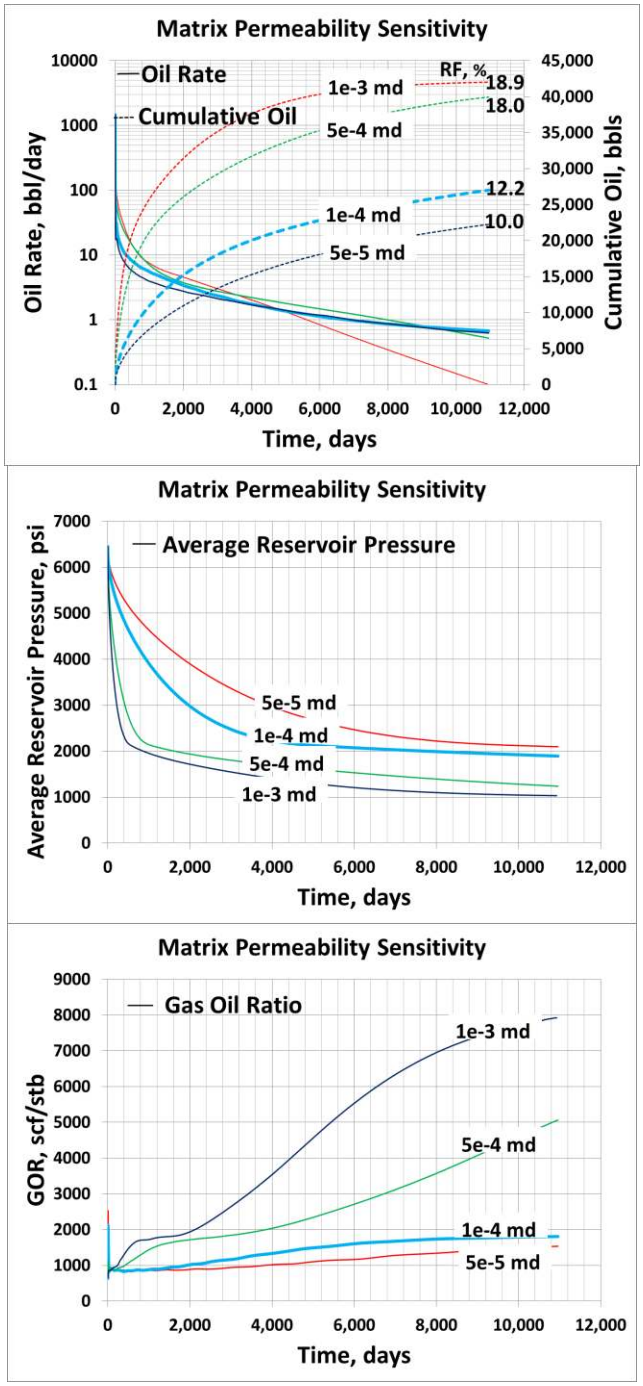

Figure 25: Matrix permeability sensitivity. Base case has fracture spacing of 200 ft, fracture half-length of 500 ft, rock compressibility of $5 \cdot 10^{-6}$ psi^{-1}, critical gas saturation of 0.05, flowing bottom-hole pressure of 1000 psi, fracture conductivity of 83.3 md-ft and matrix permeability of $1 \cdot 10^{-4}$ md

The cumulative oil production results show that the recovery at the end of 30 years of production is 10% for $5 \cdot 10^{-5}$md shale permeability but increases to 18.9 % for $1 \cdot 10^{-3}$ md shale permeability.

The average reservoir pressure also cannot be lowered much in case of $5 \cdot 10^{-5}$ md even after 30 years of production. But for $1 \cdot 10^{-3}$ md case, the reservoir pressure can be lowered to the 1,000 psi pressure limit set for the flowing bottom-hole pressure and hence the higher recovery of oil in this case. The GOR rises to a high of 8,000 scf/stb at the end of 30 years for the $1 \cdot 10^{-3}$ md case, while for other lower permeability cases; the GOR rises only slowly and stays low.

The matrix permeability is an important parameter and must be determined accurately. The recovery from the formation can be variedly different as shown in the study. Because of uncertainty in the measurement of permeability, it becomes a variable in the history matching exercise for any well.

Shale permeability can be quite difficult to quantify. Core measurements are typically orders of magnitude lower than the effective shale permeability, but a conventional formation test or buildup test is not possible with such low permeability. Mohamed, et al (2011) showed that analysis of fracture calibration tests may provide shale permeability, particularly if the test uses a very low injected volume.

This chapter illustrates sensitivity to key parameters affecting the production of the shale oil from the stimulated reservoir volume including fracture spacing, fracture half-length, rock compressibility, critical gas saturation, flowing bottom-hole pressure, hydraulic fracture conductivity and matrix permeability. The results from the sensitivity

studies can be used to design and complete better wells in the Eagle Ford shale formation leading to better well performance and higher ultimate oil recovery.

Chapter V puts a summary of the complete thesis and draws out important conclusions from the work. Also, it recommends possible future work in continuation of the work done in this thesis.

CHAPTER V

SUMMARY AND CONCLUSIONS

This chapter contains a summary of the contents of this thesis. Then we list the important conclusions of this study. Finally, we suggest ideas for future work based on the work done in this thesis.

5.1 Summary

This thesis focuses on the shale oil production from the relatively newly discovered Unconventional Eagle Ford formation. Chapter I of the thesis shows how the advancement in the technology of horizontal drilling and multi-stage hydraulic fracturing coupled with the high oil and gas prices lead to a boom in the unconventional shale oil and gas reservoirs in the recent years. The chapter also distinguishes between the commonly misunderstood terms shale oil and oil shale.

Chapter II of the thesis provides a background of the geology, mineralogy and the stimulation design for this shale formation. The chapter explains how the Eagle Ford shale is different from other shales as the Barnett and others. Eagle Ford shale produces oil, condensate and dry gas in different areas. The focus of the study is in the oil window of the Eagle Ford shale.

Chapter III explains the logarithmically gridded locally refined gridding scheme to properly model the flow in the hydraulic fracture, the flow from the fracture to the matrix and the flow in the matrix. The steep pressure and saturation changes near the hydraulic fractures are captured using this gridding scheme. At the end of the chapter,

we compare the modeled production of shale oil from the very low permeability reservoir to conventional reservoir flow behavior.

Chapter IV shows how production behavior and recovery of oil from the low permeability shale formation is a function of the rock properties, formation fluid properties and the fracturing operations. Sensitivity studies in this chapter illustrate the important parameters affecting shale oil production performance from the stimulated reservoir volume. The parameters studied in the chapter includes fracture spacing, fracture half-length, rock compressibility, critical gas saturation (for 2 phase flow below the bubble point of oil), flowing bottom-hole pressure, hydraulic fracture conductivity, and matrix permeability.

The sensitivity studies show that close fracture spacing, increased the fracture half-length, and higher fracture conductivity lead to higher recovery of oil. Further, the recovery of the oil is very sensitive to the matrix permeability.

Two phase flow below the bubble point leads to reduction in permeability for the oil and leads to lower recovery recover as gas channels through and leaves oil behind. However, oil recovery is highly sensitive to the critical gas saturation. The gas that stays in the pore spaces, before its starts moving (critical gas saturation), pushes oil out of pore spaces and leads to higher recovery.

5.2 Conclusions

Based on this study, the following conclusions can be drawn:

1. Logarithmically spaced locally refined grids capture the transient flow in the shale oil production from the stimulated reservoir volume.
2. Initial production rate from shale oil is lower in comparison to shale gas because of higher viscosity of oil in comparison to gas.
3. Designing closer fracture spacing not only leads to higher initial oil production rates but also leads to higher ultimate oil recovery factor.
4. Longer created fractures means bigger SRV and leads to higher cumulative oil production per well.
5. High sensitivity to critical gas saturation suggests that cores studies should be made to quantify this parameter.
6. Due to hydrostatic head of the oil column in the production tubing, artificial lift will necessary in all shale oil wells to lower the flowing bottom-hole pressure and boost the ultimate recovery from the well.

5.3 Recommendations

We make the following recommendations based on the work done in this thesis. First, we recommend an effort to get the actual well data, hydraulic fracturing job data, micro-seismic data, production data, production log data, build up data, PVT data and core studies data for Eagle Ford wells producing in the oil window. This would enable application of the work done in this thesis. Further, we recommend the work carried out

in this thesis for the Eagle Ford shale oil window to be applied in the Eagle Ford shale gas-condensate window. Such a study could throw some insight on the solution to the problem of condensate drop-out in the unconventional shale formations.

REFERENCES

Ahmadi, H.A.A., Almarzooq, A.M., and Wattenbarger, R.A. 2010. Application of Linear Flow Analysis to Shale Gas Wells - Field Cases. Paper SPE 130370 presented at the SPE Unconventional Gas Conference, Pittsburgh, Pennsylvania, USA, 23-25 February.

Bazan, L.W., Larkin, S.D., Lattibeaudiere, M.G., and Palisch, T.T. 2010. Improving Production in the Eagle Ford Shale with Fracture Modeling, Increased Fracture Conductivity, and Optimized Stage and Cluster Spacing Along the Horizontal Wellbore. Paper SPE 138425 presented at the Tight Gas Completions Conference, San Antonio, Texas, USA, 2-3 November.

Cipolla, C.L., Lolon, E.P., Erdle, J.C., and Rubin, B. 2010. Reservoir Modeling in Shale-Gas Reservoirs. *SPEREE* **13** (4): 638-653.

Cipolla, C.L., Warpinski, N.R., Mayerhofer, M.J., Lolon, E.P., and Vincet, M.C. 2008. The Relationship between Fracture Complexity, Reservoir Properties, and Fracture Treatment Design. Paper SPE 115769 presented at the SPE Annual Technical Conference and Exhibition, Denver, Colorado, USA, 21-24 September.

Condon, S.M. and Dyman, T.S. 2006. 2003 Geologic Assessment of Undiscovered Conventional Oil and Gas Resources in the Upper Cretaceous Navarro and Taylor Groups, Western Gulf Province, Texas: U.S. Geological Survey Digital Data Series DDS-69-H, Chapter 2 42 p. http://pubs.usgs.gov/dds/dds-069/dds-069-h/.

Energy Information Administration (EIA). 2011. Annual Energy Outlook Report 2011, http://www.eia.doe.gov/oiaf/aeo/.

Hall, H.N. 1953. Compressibility of Reservoir Rocks. *Trans*. AIME **198**: 309-311.

Holditch, S.S. 2002. The Increasing Role of Unconventional Reservoirs in the Future of the Oil and Gas Business. *JPT* **55**(11): 34-38.

Hsu, S.-C. and Nelson, P.P. 2002. Characterization of Eagle Ford Shale. *Engineering Geology* **67** (1-2): 169-183.

Masters, J.A. 1979. Deep Basin Gas Trap, Western Canada. *AAPG* **63**(2): 152.

Mayerhofer, M.J., Lolon, E.P., Youngblood, J.E., and Heinze, J.R. 2006. Integration of Microseismic-Fracture-Mapping Results with Numerical Fracture Network Production Modeling in the Barnett Shale. Paper SPE 102103 presented at the SPE Annual Technical Conference and Exhibition, San Antonio, Texas, USA, 24-27 September.

Miskimins, J.L. 2008. Design and Life Cycle Considerations for Unconventional Reservoir Wells. Paper SPE 114170 presented at the SPE Unconventional Reservoirs Conference, Keystone, Colorado, USA, 10-12 February.

Mohamed, I.M., Nasralla, R.A., Sayed, M.A., Marongiu-Porcu, M., and Ehlig-Economides, C.A. 2011. Evaluation of after-Closure Analysis Techniques for Tight and Shale Gas Formations. Paper SPE 140136 presented at the SPE Hydraulic Fracturing Technology Conference, The Woodlands, Texas, USA, 24-26 January.

Mullen, J., Lowry, J. C., and Nwabuoku, K.C. (2010). Lessons Learned Developing the Eagle Ford Shale. Paper SPE 138446 presented at the Tight Gas Completions Conference. San Antonio, Texas, USA, 2-3 November.

Passey, Q. R., Bohacs, K.M., Esch, W.L., Klimentidis, R., and Sinha, S. (2010). From Oil-Prone Source Rock to Gas-Producing Shale Reservoir - Geologic and Petrophysical Characterization of Unconventional Shale Gas Reservoirs. Paper SPE 131350 presented at the International Oil and Gas Conference and Exhibition in China. Beijing, China, 8-10 june.

Rickman, R., Mullen, M.J., Petre, J.E., Grieser, B., and Kundert, D. 2008. A Practical Use of Shale Petrophysics for Stimulation Design Optimization: All Shale Plays Are Not Clones of the Barnett Shale. Paper SPE 115258 presented at the SPE Annual Technical Conference and Exhibition, Denver, Colorado, USA, 21-24 September.

Rubin, B. 2010. Accurate Simulation of Non Darcy Flow in Stimulated Fractured Shale Reservoirs. Paper SPE 132093 presented at the SPE Western Regional Meeting, Anaheim, California, USA, 27-29 May.

Song, B., Economides, M.J., and Ehlig-Economides, C. 2011. Design of Multiple Transverse Fracture Horizontal Wells in Shale Gas Reservoirs. Paper SPE 140555 presented at the SPE Hydraulic Fracturing Technology Conference. The Woodlands, Texas, USA, 24-26 January.

Stegent, N. A., Wagner, A.L., Mullen, J., and Borstmayer, R.E. 2010. Engineering a Successful Fracture-Stimulation Treatment in the Eagle Ford Shale. Paper SPE

136183 presented at the Tight Gas Completions Conference. San Antonio, Texas, USA, 2-3 November.

Supplemental Sources Consulted

Ahmed, T.: *Reservoir Engineering Handbook,* Gulf Professional Publishing, Houston, Texas, 2001.

Corey, A.T. 1954. The Interrelation between Gas and Oil Relative Permeabilities. Producers Monthly (November, 1954): 38-41.A.T. Corey, A.T. 1954.

Etherington, J. R. and McDonald, I. R. (2004). Is Bitumen a Petroleum Reserve? Paper SPE 90242 presented at the SPE Annual Technical Conference and Exhibition. Houston, Texas, 26-29 September.

Mayerhofer, M.J., Lolon, E.P., Warpinski, N.R., Cipolla, C.L., Walser, D., and Rightmire, C.M. 2010. What Is Stimulated Reservoir Volume? *SPE PO* **25** (1) 89-98.

Mullen, J. (2010). Petrophysical Characterization of the Eagle Ford Shale in South Texas. Paper SPE 138145 presented at the Canadian Unconventional Resources and International Petroleum Conference. Calgary, Alberta, Canada, 19-21 October.

Orangi, A., Nagarajan, N. R., Honarpour, M.M., and Rosenzweig, J. (2011). Unconventional Shale Oil and Gas-Condensate Reservoir Production, Impact of Rock, Fluid, and Hydraulic Fractures. Paper SPE 140536 presented at the

SPE Hydraulic Fracturing Technology Conference. The Woodlands, Texas, USA, 24-26 January.

Rahmanian, M.R., Solano, N., and Aguilera, R. 2010. Storage and Output Flow from Shale and Tight Gas Reservoirs. Paper SPE 133611 presented at the SPE Western Regional Meeting, Anaheim, California, USA, 27-29 May.

Vassilellis, G. D., Li, C., Seager, R., and Moos, D. 2010. Investigating the Expected Long-Term Production Performance of Shale Reservoirs. Paper SPE 138134 presented at the Canadian Unconventional Resources and International Petroleum Conference. Calgary, Alberta, Canada, 19-21 October.

APPENDIX

BASE CASE SIMULATION CMG INPUT FILE

```
RESULTS SIMULATOR IMEX 200900


INTERRUPT RESTART-STOP


INUNIT FIELD
WSRF WELL 1
WSRF GRID TIME
WSRF SECTOR TIME
OUTSRF WELL LAYER NONE
OUTSRF RES ALL
OUTSRF GRID BPP KRG KRO KRW PRES SG SO SSPRES SW VISG VISO
        WINFLUX
WPRN GRID 0
OUTPRN GRID NONE
OUTPRN RES NONE
**$  Distance units: ft
RESULTS XOFFSET         0.0000
RESULTS YOFFSET         0.0000
RESULTS ROTATION          0.0000  **$  (DEGREES)
RESULTS AXES-DIRECTIONS 1.0 -1.0 1.0
**$
**********************************************************************
****
**$ Definition of fundamental cartesian grid
**$
**********************************************************************
****
GRID VARI 1 5 1
KDIR DOWN
DI IVAR
 200
DJ JVAR
 5*200
DK ALL
 5*200
DTOP
 5*9884
REFINE 1,5,1 INTO 49 11 1
```

```
DI RG 1,5,1 IVAR
 17.45958 14.41121 11.89507 9.818244 8.10402 6.689092 5.521204 4.557225
 3.761553 3.104801 2.562716 2.115277 1.745958 1.441121 1.189507 0.9818244
 0.810402 0.6689092 0.5521204 0.4557225 0.3761553 0.3104801 0.2562716
 0.2115277 2 0.2115277 0.2562716 0.3104801 0.3761553 0.4557225 0.5521204
 0.6689092 0.810402 0.9818244 1.189507 1.441121 1.745958 2.115277 2.562716
 3.104801 3.761553 4.557225 5.521204 6.689092 8.10402 9.818244 11.89507
 14.41121 17.45958
REFINE 1,4,1 INTO 49 11 1

DI RG 1,4,1 IVAR
 17.45958 14.41121 11.89507 9.818244 8.10402 6.689092 5.521204 4.557225
 3.761553 3.104801 2.562716 2.115277 1.745958 1.441121 1.189507 0.9818244
 0.810402 0.6689092 0.5521204 0.4557225 0.3761553 0.3104801 0.2562716
 0.2115277 2 0.2115277 0.2562716 0.3104801 0.3761553 0.4557225 0.5521204
 0.6689092 0.810402 0.9818244 1.189507 1.441121 1.745958 2.115277 2.562716
 3.104801 3.761553 4.557225 5.521204 6.689092 8.10402 9.818244 11.89507
 14.41121 17.45958
REFINE 1,1,1 INTO 49 11 1

DI RG 1,1,1 IVAR
 17.45958 14.41121 11.89507 9.818244 8.10402 6.689092 5.521204 4.557225
 3.761553 3.104801 2.562716 2.115277 1.745958 1.441121 1.189507 0.9818244
 0.810402 0.6689092 0.5521204 0.4557225 0.3761553 0.3104801 0.2562716
 0.2115277 2 0.2115277 0.2562716 0.3104801 0.3761553 0.4557225 0.5521204
 0.6689092 0.810402 0.9818244 1.189507 1.441121 1.745958 2.115277 2.562716
 3.104801 3.761553 4.557225 5.521204 6.689092 8.10402 9.818244 11.89507
 14.41121 17.45958
REFINE 1,2,1 INTO 49 11 1

DI RG 1,2,1 IVAR
 17.45958 14.41121 11.89507 9.818244 8.10402 6.689092 5.521204 4.557225
 3.761553 3.104801 2.562716 2.115277 1.745958 1.441121 1.189507 0.9818244
 0.810402 0.6689092 0.5521204 0.4557225 0.3761553 0.3104801 0.2562716
 0.2115277 2 0.2115277 0.2562716 0.3104801 0.3761553 0.4557225 0.5521204
 0.6689092 0.810402 0.9818244 1.189507 1.441121 1.745958 2.115277 2.562716
 3.104801 3.761553 4.557225 5.521204 6.689092 8.10402 9.818244 11.89507
 14.41121 17.45958
REFINE 1,3,1 INTO 49 49 1

DI RG 1,3,1 IVAR
 17.45958 14.41121 11.89507 9.818244 8.10402 6.689092 5.521204 4.557225
 3.761553 3.104801 2.562716 2.115277 1.745958 1.441121 1.189507 0.9818244
```

```
 0.810402 0.6689092 0.5521204 0.4557225 0.3761553 0.3104801 0.2562716
 0.2115277 2 0.2115277 0.2562716 0.3104801 0.3761553 0.4557225 0.5521204
 0.6689092 0.810402 0.9818244 1.189507 1.441121 1.745958 2.115277 2.562716
 3.104801 3.761553 4.557225 5.521204 6.689092 8.10402 9.818244 11.89507
 14.41121 17.45958
DJ RG 1,3,1 JVAR
 17.45958 14.41121 11.89507 9.818244 8.10402 6.689092 5.521204 4.557225
 3.761553 3.104801 2.562716 2.115277 1.745958 1.441121 1.189507 0.9818244
 0.810402 0.6689092 0.5521204 0.4557225 0.3761553 0.3104801 0.2562716
 0.2115277 2 0.2115277 0.2562716 0.3104801 0.3761553 0.4557225 0.5521204
 0.6689092 0.810402 0.9818244 1.189507 1.441121 1.745958 2.115277 2.562716
 3.104801 3.761553 4.557225 5.521204 6.689092 8.10402 9.818244 11.89507
 14.41121 17.45958
**$ Property: Permeability I (md)   Max: 0.0001  Min: 0.0001
**$ Property: Permeability I (md)   Max: 41.65  Min: 0.0001
PERMI CON       0.0001
PERMI RG 1,5,1 ALL
 24*0.0001 41.65 48*0.0001 41.65 48*0.0001 41.65 48*0.0001 41.65 48*0.0001
 41.65 48*0.0001 41.65 48*0.0001 41.65 48*0.0001 41.65 48*0.0001 41.65
 48*0.0001 41.65 48*0.0001 41.65 24*0.0001
PERMI RG 1,4,1 ALL
 24*0.0001 41.65 48*0.0001 41.65 48*0.0001 41.65 48*0.0001 41.65 48*0.0001
 41.65 48*0.0001 41.65 48*0.0001 41.65 48*0.0001 41.65 48*0.0001 41.65
 48*0.0001 41.65 48*0.0001 41.65 24*0.0001
PERMI RG 1,1,1 ALL
 24*0.0001 41.65 48*0.0001 41.65 48*0.0001 41.65 48*0.0001 41.65 48*0.0001
 41.65 48*0.0001 41.65 48*0.0001 41.65 48*0.0001 41.65 48*0.0001 41.65
 48*0.0001 41.65 48*0.0001 41.65 24*0.0001
PERMI RG 1,2,1 ALL
 24*0.0001 41.65 48*0.0001 41.65 48*0.0001 41.65 48*0.0001 41.65 48*0.0001
 41.65 48*0.0001 41.65 48*0.0001 41.65 48*0.0001 41.65 48*0.0001 41.65
 48*0.0001 41.65 48*0.0001 41.65 24*0.0001
PERMI RG 1,3,1 ALL
 24*0.0001 41.65 48*0.0001 41.65 48*0.0001 41.65 48*0.0001 41.65 48*0.0001
 41.65 48*0.0001 41.65 48*0.0001 41.65 48*0.0001 41.65 48*0.0001 41.65
 48*0.0001 41.65 48*0.0001 41.65 48*0.0001 41.65 48*0.0001 41.65 48*0.0001
 41.65 48*0.0001 41.65 48*0.0001 41.65 48*0.0001 41.65 48*0.0001 41.65
 48*0.0001 41.65 48*0.0001 41.65 48*0.0001 41.65 48*0.0001 41.65 48*0.0001
 41.65 48*0.0001 41.65 48*0.0001 41.65 48*0.0001 41.65 48*0.0001 41.65
 48*0.0001 41.65 48*0.0001 41.65 48*0.0001 41.65 48*0.0001 41.65 48*0.0001
 41.65 48*0.0001 41.65 48*0.0001 41.65 48*0.0001 41.65 48*0.0001 41.65
 48*0.0001 41.65 48*0.0001 41.65 48*0.0001 41.65 48*0.0001 41.65 48*0.0001
 41.65 48*0.0001 41.65 48*0.0001 41.65 48*0.0001 41.65 48*0.0001 41.65
 48*0.0001 41.65 48*0.0001 41.65 48*0.0001 41.65 48*0.0001 41.65 24*0.0001
```

```
**$ Property: NULL Blocks  Max: 1  Min: 1
**$  0 = null block, 1 = active block
**$  0 = null block, 1 = active block
NULL CON           1
**$ Property: Porosity  Max: 0.06  Min: 0.06
POR CON         0.06
**$ Property: Permeability J (md)   Max: 0.0001  Min: 0.0001
**$ Property: Permeability J (md)   Max: 41.65  Min: 0.0001
PERMJ CON       0.0001
PERMJ RG 1,5,1 ALL
 24*0.0001 41.65 48*0.0001 41.65 48*0.0001 41.65 48*0.0001 41.65 48*0.0001
 41.65 48*0.0001 41.65 48*0.0001 41.65 48*0.0001 41.65 48*0.0001 41.65
 48*0.0001 41.65 48*0.0001 41.65 24*0.0001
PERMJ RG 1,4,1 ALL
 24*0.0001 41.65 48*0.0001 41.65 48*0.0001 41.65 48*0.0001 41.65 48*0.0001
 41.65 48*0.0001 41.65 48*0.0001 41.65 48*0.0001 41.65 48*0.0001 41.65
 48*0.0001 41.65 48*0.0001 41.65 24*0.0001
PERMJ RG 1,1,1 ALL
 24*0.0001 41.65 48*0.0001 41.65 48*0.0001 41.65 48*0.0001 41.65 48*0.0001
 41.65 48*0.0001 41.65 48*0.0001 41.65 48*0.0001 41.65 48*0.0001 41.65
 48*0.0001 41.65 48*0.0001 41.65 24*0.0001
PERMJ RG 1,2,1 ALL
 24*0.0001 41.65 48*0.0001 41.65 48*0.0001 41.65 48*0.0001 41.65 48*0.0001
 41.65 48*0.0001 41.65 48*0.0001 41.65 48*0.0001 41.65 48*0.0001 41.65
 48*0.0001 41.65 48*0.0001 41.65 24*0.0001
PERMJ RG 1,3,1 ALL
 24*0.0001 41.65 48*0.0001 41.65 48*0.0001 41.65 48*0.0001 41.65 48*0.0001
 41.65 48*0.0001 41.65 48*0.0001 41.65 48*0.0001 41.65 48*0.0001 41.65
 48*0.0001 41.65 48*0.0001 41.65 48*0.0001 41.65 48*0.0001 41.65 48*0.0001
 41.65 48*0.0001 41.65 48*0.0001 41.65 48*0.0001 41.65 48*0.0001 41.65
 48*0.0001 41.65 48*0.0001 41.65 48*0.0001 41.65 48*0.0001 41.65 48*0.0001
 41.65 48*0.0001 41.65 48*0.0001 41.65 48*0.0001 41.65 48*0.0001 41.65
 48*0.0001 41.65 48*0.0001 41.65 48*0.0001 41.65 48*0.0001 41.65 48*0.0001
 41.65 48*0.0001 41.65 48*0.0001 41.65 48*0.0001 41.65 48*0.0001 41.65
 48*0.0001 41.65 48*0.0001 41.65 48*0.0001 41.65 48*0.0001 41.65 48*0.0001
 41.65 48*0.0001 41.65 48*0.0001 41.65 48*0.0001 41.65 48*0.0001 41.65
 48*0.0001 41.65 48*0.0001 41.65 48*0.0001 41.65 48*0.0001 41.65 24*0.0001
**$ Property: Permeability K (md)   Max: 0.0001  Min: 0.0001
**$ Property: Permeability K (md)   Max: 41.65  Min: 0.0001
PERMK CON       0.0001
PERMK RG 1,5,1 ALL
 24*0.0001 41.65 48*0.0001 41.65 48*0.0001 41.65 48*0.0001 41.65 48*0.0001
 41.65 48*0.0001 41.65 48*0.0001 41.65 48*0.0001 41.65 48*0.0001 41.65
 48*0.0001 41.65 48*0.0001 41.65 24*0.0001
```

```
PERMK RG 1,4,1 ALL
 24*0.0001 41.65 48*0.0001 41.65 48*0.0001 41.65 48*0.0001 41.65 48*0.0001
 41.65 48*0.0001 41.65 48*0.0001 41.65 48*0.0001 41.65 48*0.0001 41.65
 48*0.0001 41.65 48*0.0001 41.65 24*0.0001
PERMK RG 1,1,1 ALL
 24*0.0001 41.65 48*0.0001 41.65 48*0.0001 41.65 48*0.0001 41.65 48*0.0001
 41.65 48*0.0001 41.65 48*0.0001 41.65 48*0.0001 41.65 48*0.0001 41.65
 48*0.0001 41.65 48*0.0001 41.65 24*0.0001
PERMK RG 1,2,1 ALL
 24*0.0001 41.65 48*0.0001 41.65 48*0.0001 41.65 48*0.0001 41.65 48*0.0001
 41.65 48*0.0001 41.65 48*0.0001 41.65 48*0.0001 41.65 48*0.0001 41.65
 48*0.0001 41.65 48*0.0001 41.65 24*0.0001
PERMK RG 1,3,1 ALL
 24*0.0001 41.65 48*0.0001 41.65 48*0.0001 41.65 48*0.0001 41.65 48*0.0001
 41.65 48*0.0001 41.65 48*0.0001 41.65 48*0.0001 41.65 48*0.0001 41.65
 48*0.0001 41.65 48*0.0001 41.65 48*0.0001 41.65 48*0.0001 41.65 48*0.0001
 41.65 48*0.0001 41.65 48*0.0001 41.65 48*0.0001 41.65 48*0.0001 41.65
 48*0.0001 41.65 48*0.0001 41.65 48*0.0001 41.65 48*0.0001 41.65 48*0.0001
 41.65 48*0.0001 41.65 48*0.0001 41.65 48*0.0001 41.65 48*0.0001 41.65
 48*0.0001 41.65 48*0.0001 41.65 48*0.0001 41.65 48*0.0001 41.65 48*0.0001
 41.65 48*0.0001 41.65 48*0.0001 41.65 48*0.0001 41.65 48*0.0001 41.65
 48*0.0001 41.65 48*0.0001 41.65 48*0.0001 41.65 48*0.0001 41.65 48*0.0001
 41.65 48*0.0001 41.65 48*0.0001 41.65 48*0.0001 41.65 48*0.0001 41.65
 48*0.0001 41.65 48*0.0001 41.65 48*0.0001 41.65 48*0.0001 41.65 24*0.0001
**$ Property: Pinchout Array  Max: 1  Min: 1
**$  0 = pinched block, 1 = active block
**$  0 = pinched block, 1 = active block
PINCHOUTARRAY CON           1
PRPOR 5000
CPOR 5e-6
MODEL BLACKOIL
TRES 255
PVT EG 1

**$        p          Rs        Bo        Eg      viso       visg
     14.696     4.68138   1.09917   4.10159  0.902644  0.0136014
    173.583     32.1923   1.11173   49.1225  0.803844  0.0137243
     332.47     65.2796   1.12711   95.3676  0.719427  0.0139054
    491.357     101.621    1.1443   142.801  0.651788  0.0141273
    650.244      140.36   1.16295   191.364   0.59727   0.014385
    809.131     181.027   1.18287   240.971  0.552597  0.0146766
    968.018      223.32   1.20393   291.506  0.515357  0.0150009
     1126.9     267.027   1.22604   342.824  0.483819  0.0153574
    1285.79     311.989   1.24913    394.75   0.45674  0.0157453
```

```
     1444.68     358.084   1.27314   447.084  0.433209  0.0161637
     1603.57     405.212   1.29803   499.604  0.412545  0.0166117
     1762.45     453.293   1.32376   552.077  0.394234  0.0170877
     1921.34     502.257    1.3503   604.264  0.377877  0.0175899
     2080.23     552.048    1.3776   655.935  0.363163  0.0181162
     2239.11     602.616   1.40566   706.874  0.349843  0.0186643
        2398     653.915   1.43443   756.888  0.337718  0.0192317
      3218.4     929.142   1.59372   995.379  0.288941  0.0223706
      4038.8     1219.15   1.76935   1195.74  0.255067  0.0256431
      4859.2     1521.47   1.95964   1360.49  0.229917  0.0288538
      5679.6     1834.43   2.16332   1496.29   0.21036  0.0319135
        6500  2193.142554   2.37939   1609.67   0.19463  0.0347948
GRAVITY GAS 0.8
REFPW 14.696
DENSITY WATER 59.1613
BWI 1.06212
CW 3.72431e-006
VWI 0.23268
CVW 0.0
**$ Property: PVT Type  Max: 1  Min: 1
PTYPE CON           1
DENSITY OIL 50.863
CO 1e-5
ROCKFLUID
RPT 1 SCALING-OLD
**$       Sw          krw         krow
SWT
         0.3           0           1
       0.325  9.53674e-007    0.724196
        0.35  3.05176e-005    0.512909
       0.375  0.000231743     0.354093
         0.4  0.000976562     0.237305
       0.425   0.00298023      0.15359
        0.45   0.00741577    0.0953674
       0.475    0.0160284    0.0563135
         0.5      0.03125      0.03125
       0.525    0.0563135    0.0160284
        0.55    0.0953674   0.00741577
       0.575     0.15359   0.00298023
         0.6    0.237305  0.000976563
       0.625     0.354093  0.000231743
        0.65     0.512909 3.05176e-005
       0.675     0.724196 9.53674e-007
         0.7            1           0
```

```
**$       Sl        krg         krog
SLT
        0.6         1           0
    0.621875    0.878906  9.53674e-007
     0.64375    0.765625  3.05176e-005
    0.665625    0.660156   0.000231743
      0.6875      0.5625   0.000976563
    0.709375    0.472656    0.00298023
     0.73125    0.390625    0.00741577
    0.753125    0.316406     0.0160284
       0.775        0.25       0.03125
    0.796875    0.191406     0.0563135
     0.81875    0.140625     0.0953674
    0.840625   0.0976562       0.15359
      0.8625      0.0625      0.237305
    0.884375   0.0351562      0.354093
     0.90625    0.015625      0.512909
    0.928125  0.00390625      0.724196
        0.95           0           1
RPT 2 SCALING-OLD
**$       Sw        krw       krow
SWT
        0.05          0          1
    0.103125   0.015625    0.90773
     0.15625  0.0441942   0.818488
    0.209375  0.0811899   0.732378
      0.2625      0.125   0.649519
    0.315625   0.174693   0.570045
     0.36875    0.22964   0.494106
    0.421875   0.289379   0.421875
       0.475   0.353553   0.353553
    0.528125   0.421875   0.289379
     0.58125   0.494106    0.22964
    0.634375   0.570045   0.174693
      0.6875   0.649519      0.125
    0.740625   0.732378  0.0811899
     0.79375   0.818488  0.0441942
    0.846875    0.90773   0.015625
         0.9          1          0
**$       Sl       krg       krog
SLT
        0.15         1          0
    0.203125    0.9375   0.015625
     0.25625     0.875  0.0441942
```

```
    0.309375    0.8125  0.0811899
     0.3625      0.75      0.125
    0.415625    0.6875   0.174693
     0.46875     0.625    0.22964
    0.521875    0.5625   0.289379
       0.575       0.5   0.353553
    0.628125    0.4375   0.421875
     0.68125     0.375   0.494106
    0.734375    0.3125   0.570045
      0.7875      0.25   0.649519
    0.840625    0.1875   0.732378
     0.89375     0.125   0.818488
    0.946875    0.0625    0.90773
           1         0         1
RTYPE RG 1,4,1 ALL
 24*1 2 48*1 2 48*1 2 48*1 2 48*1 2 48*1 2 48*1 2 48*1 2 48*1 2 48*1 2 48*1
 2 48*1 2 24*1
RTYPE RG 1,1,1 ALL
 24*1 2 48*1 2 48*1 2 48*1 2 48*1 2 48*1 2 48*1 2 48*1 2 48*1 2 48*1 2 48*1
 2 48*1 2 24*1
RTYPE RG 1,2,1 ALL
 24*1 2 48*1 2 48*1 2 48*1 2 48*1 2 48*1 2 48*1 2 48*1 2 48*1 2 48*1 2 48*1
 2 48*1 2 24*1
RTYPE RG 1,3,1 ALL
 24*1 2 48*1 2 48*1 2 48*1 2 48*1 2 48*1 2 48*1 2 48*1 2 48*1 2 48*1 2 48*1
 2 48*1 2 48*1 2 48*1 2 48*1 2 48*1 2 48*1 2 48*1 2 48*1 2 48*1 2 48*1 2 48*1
 2 48*1 2 48*1 2 48*1 2 48*1 2 48*1 2 48*1 2 48*1 2 48*1 2 48*1 2 48*1 2 48*1
 2 48*1 2 48*1 2 48*1 2 48*1 2 48*1 2 48*1 2 48*1 2 48*1 2 48*1 2 48*1 2 48*1
 2 48*1 2 48*1 2 48*1 2 48*1 2 48*1 2 48*1 2 48*1 2 48*1 2 48*1 2 48*1 2 24*1
**$ Property: Rel Perm Set Num  Max: 2  Min: 1
RTYPE CON           1
RTYPE RG 1,5,1 ALL
 24*1 2 48*1 2 48*1 2 48*1 2 48*1 2 48*1 2 48*1 2 48*1 2 48*1 2 48*1 2 48*1
 2 48*1 2 24*1
RTYPE RG 1,4,1 ALL
 24*1 2 48*1 2 48*1 2 48*1 2 48*1 2 48*1 2 48*1 2 48*1 2 48*1 2 48*1 2 48*1
 2 48*1 2 24*1
RTYPE RG 1,1,1 ALL
 24*1 2 48*1 2 48*1 2 48*1 2 48*1 2 48*1 2 48*1 2 48*1 2 48*1 2 48*1 2 48*1
 2 48*1 2 24*1
RTYPE RG 1,2,1 ALL
 24*1 2 48*1 2 48*1 2 48*1 2 48*1 2 48*1 2 48*1 2 48*1 2 48*1 2 48*1 2 48*1
 2 48*1 2 24*1
RTYPE RG 1,3,1 ALL
```

```
 24*1 2 48*1 2 48*1 2 48*1 2 48*1 2 48*1 2 48*1 2 48*1 2 48*1 2 48*1
 2 48*1 2 48*1 2 48*1 2 48*1 2 48*1 2 48*1 2 48*1 2 48*1 2 48*1 2 48*1
 2 48*1 2 48*1 2 48*1 2 48*1 2 48*1 2 48*1 2 48*1 2 48*1 2 48*1 2 48*1
 2 48*1 2 48*1 2 48*1 2 48*1 2 48*1 2 48*1 2 48*1 2 48*1 2 48*1 2 48*1
 2 48*1 2 48*1 2 48*1 2 48*1 2 48*1 2 48*1 2 48*1 2 48*1 2 48*1 2 24*1
**$ Property: Rel Perm Set Num  Max: 2  Min: 1
RTYPE CON           1
RTYPE RG 1,5,1 ALL
 24*1 2 48*1 2 48*1 2 48*1 2 48*1 2 48*1 2 48*1 2 48*1 2 48*1 2 48*1
 2 48*1 2 24*1
RTYPE RG 1,4,1 ALL
 24*1 2 48*1 2 48*1 2 48*1 2 48*1 2 48*1 2 48*1 2 48*1 2 48*1 2 48*1
 2 48*1 2 24*1
RTYPE RG 1,1,1 ALL
 24*1 2 48*1 2 48*1 2 48*1 2 48*1 2 48*1 2 48*1 2 48*1 2 48*1 2 48*1
 2 48*1 2 24*1
RTYPE RG 1,2,1 ALL
 24*1 2 48*1 2 48*1 2 48*1 2 48*1 2 48*1 2 48*1 2 48*1 2 48*1 2 48*1
 2 48*1 2 24*1
RTYPE RG 1,3,1 ALL
 24*1 2 48*1 2 48*1 2 48*1 2 48*1 2 48*1 2 48*1 2 48*1 2 48*1 2 48*1
 2 48*1 2 48*1 2 48*1 2 48*1 2 48*1 2 48*1 2 48*1 2 48*1 2 48*1 2 48*1
 2 48*1 2 48*1 2 48*1 2 48*1 2 48*1 2 48*1 2 48*1 2 48*1 2 48*1 2 48*1
 2 48*1 2 48*1 2 48*1 2 48*1 2 48*1 2 48*1 2 48*1 2 48*1 2 48*1 2 48*1
 2 48*1 2 48*1 2 48*1 2 48*1 2 48*1 2 48*1 2 48*1 2 48*1 2 48*1 2 24*1
**$ Property: Forchheimer Equation Beta Correction  Max: 0  Min: 0
NDARCYCOR CON           0
INITIAL
VERTICAL DEPTH_AVE WATER_OIL EQUIL

REFDEPTH 9884
REFPRES 6425
DWOC 15000
**$ Property: Bubble Point Pressure (psi)   Max: 2398  Min: 2398
PB CON        2398
NUMERICAL
DTMIN 1e-9
NORTH 40
ITERMAX 100
RUN
DATE 2010 1 1
DTWELL 1e-008
**$
WELL  '1'
```

```
PRODUCER '1'
OPERATE  MIN  BHP  1000.  CONT
**$ UBA    ff  Status  Connection
**$         rad  geofac  wfrac  skin
GEOMETRY  J  0.25  0.37  1.  0.
PERF  GEOA  '1'
**$ UBA             ff  Status  Connection
   1 3 1 / 25 25 1  1.  OPEN    FLOW-TO  'SURFACE'
**$ Property: Implicit flag  Max: 1  Min: 1
AIMSET   *CON 1
DATE 2010 1  1.04167
DATE 2010 1  1.08333
DATE 2010 1  1.12500
DATE 2010 1  1.16667
DATE 2010 1  1.20833
DATE 2010 1  1.25000
DATE 2010 1  1.29167
DATE 2010 1  1.33333
DATE 2010 1  1.37500
DATE 2010 1  1.41667
DATE 2010 1  1.45833
DATE 2010 1  1.50000
DATE 2010 1  1.54167
DATE 2010 1  1.58333
DATE 2010 1  1.62500
DATE 2010 1  1.66667
DATE 2010 1  1.70833
DATE 2010 1  1.75000
DATE 2010 1  1.79167
DATE 2010 1  1.83333
DATE 2010 1  1.87500
DATE 2010 1  1.91667
DATE 2010 1  1.95833
DATE 2010 1  2.00000
DATE 2010 1  2.08333
DATE 2010 1  2.16667
DATE 2010 1  2.25000
DATE 2010 1  2.33333
DATE 2010 1  2.41667
DATE 2010 1  2.50000
DATE 2010 1  2.58333
DATE 2010 1  2.66667
DATE 2010 1  2.75000
DATE 2010 1  2.83333
```

DATE 2010 1 2.91667
DATE 2010 1 3.00000
DATE 2010 1 3.12500
DATE 2010 1 3.25000
DATE 2010 1 3.37500
DATE 2010 1 3.50000
DATE 2010 1 3.62500
DATE 2010 1 3.75000
DATE 2010 1 3.87500
DATE 2010 1 4.00000
DATE 2010 1 5.00000
DATE 2010 1 6.00000
DATE 2010 1 7.00000
DATE 2010 1 8.00000
DATE 2010 1 9.00000
DATE 2010 1 10.00000
DATE 2010 1 11.00000
DATE 2010 1 12.00000
DATE 2010 1 13.00000
DATE 2010 1 14.00000
DATE 2010 1 15.00000
DATE 2010 1 16.00000
DATE 2010 1 17.00000
DATE 2010 1 18.00000
DATE 2010 1 19.00000
DATE 2010 1 20.00000
DATE 2010 1 21.00000
DATE 2010 1 22.00000
DATE 2010 1 23.00000
DATE 2010 1 24.00000
DATE 2010 1 25.00000
DATE 2010 1 26.00000
DATE 2010 1 27.00000
DATE 2010 1 28.00000
DATE 2010 1 29.00000
DATE 2010 1 30.00000
DATE 2010 1 31.00000
DATE 2010 2 1.00000
DATE 2010 3 1.00000
DATE 2010 4 1.00000
DATE 2010 5 1.00000
DATE 2010 6 1.00000
DATE 2010 7 1.00000
DATE 2010 8 1.00000

DATE 2010 9 1.00000
DATE 2010 10 1.00000
DATE 2010 11 1.00000
DATE 2010 12 1.00000

DATE 2011 1 1.00000
DATE 2011 2 1.00000
DATE 2011 3 1.00000
DATE 2011 4 1.00000
DATE 2011 5 1.00000
DATE 2011 6 1.00000
DATE 2011 7 1.00000
DATE 2011 8 1.00000
DATE 2011 9 1.00000
DATE 2011 10 1.00000
DATE 2011 11 1.00000
DATE 2011 12 1.00000

DATE 2012 1 1.00000
DATE 2012 2 1.00000
DATE 2012 3 1.00000
DATE 2012 4 1.00000
DATE 2012 5 1.00000
DATE 2012 6 1.00000
DATE 2012 7 1.00000
DATE 2012 8 1.00000
DATE 2012 9 1.00000
DATE 2012 10 1.00000
DATE 2012 11 1.00000
DATE 2012 12 1.00000
DATE 2013 1 1.00000
DATE 2013 2 1.00000
DATE 2013 3 1.00000
DATE 2013 4 1.00000
DATE 2013 5 1.00000
DATE 2013 6 1.00000
DATE 2013 7 1.00000
DATE 2013 8 1.00000
DATE 2013 9 1.00000
DATE 2013 10 1.00000
DATE 2013 11 1.00000
DATE 2013 12 1.00000
DATE 2014 1 1.00000
DATE 2014 2 1.00000

DATE 2014 3 1.00000
DATE 2014 4 1.00000
DATE 2014 5 1.00000
DATE 2014 6 1.00000
DATE 2014 7 1.00000
DATE 2014 8 1.00000
DATE 2014 9 1.00000
DATE 2014 10 1.00000
DATE 2014 11 1.00000
DATE 2014 12 1.00000
DATE 2015 1 1.00000
DATE 2015 2 1.00000
DATE 2015 3 1.00000
DATE 2015 4 1.00000
DATE 2015 5 1.00000
DATE 2015 6 1.00000
DATE 2015 7 1.00000
DATE 2015 8 1.00000
DATE 2015 9 1.00000
DATE 2015 10 1.00000
DATE 2015 11 1.00000
DATE 2015 12 1.00000
DATE 2016 1 1.00000
DATE 2016 2 1.00000
DATE 2016 3 1.00000
DATE 2016 4 1.00000
DATE 2016 5 1.00000
DATE 2016 6 1.00000
DATE 2016 7 1.00000
DATE 2016 8 1.00000
DATE 2016 9 1.00000
DATE 2016 10 1.00000
DATE 2016 11 1.00000
DATE 2016 12 1.00000
DATE 2017 1 1.00000
DATE 2017 2 1.00000
DATE 2017 3 1.00000
DATE 2017 4 1.00000
DATE 2017 5 1.00000
DATE 2017 6 1.00000
DATE 2017 7 1.00000
DATE 2017 8 1.00000
DATE 2017 9 1.00000
DATE 2017 10 1.00000

DATE 2017 11 1.00000
DATE 2017 12 1.00000
DATE 2018 1 1.00000
DATE 2018 2 1.00000
DATE 2018 3 1.00000
DATE 2018 4 1.00000
DATE 2018 5 1.00000
DATE 2018 6 1.00000
DATE 2018 7 1.00000
DATE 2018 8 1.00000
DATE 2018 9 1.00000
DATE 2018 10 1.00000
DATE 2018 11 1.00000
DATE 2018 12 1.00000
DATE 2019 1 1.00000
DATE 2019 2 1.00000
DATE 2019 3 1.00000
DATE 2019 4 1.00000
DATE 2019 5 1.00000
DATE 2019 6 1.00000
DATE 2019 7 1.00000
DATE 2019 8 1.00000
DATE 2019 9 1.00000
DATE 2019 10 1.00000
DATE 2019 11 1.00000
DATE 2019 12 1.00000
DATE 2020 1 1.00000
DATE 2020 2 1.00000
DATE 2020 3 1.00000
DATE 2020 4 1.00000
DATE 2020 5 1.00000
DATE 2020 6 1.00000
DATE 2020 7 1.00000
DATE 2020 8 1.00000
DATE 2020 9 1.00000
DATE 2020 10 1.00000
DATE 2020 11 1.00000
DATE 2020 12 1.00000
DATE 2021 1 1.00000
DATE 2021 2 1.00000
DATE 2021 3 1.00000
DATE 2021 4 1.00000
DATE 2021 5 1.00000
DATE 2021 6 1.00000

DATE 2021 7 1.00000
DATE 2021 8 1.00000
DATE 2021 9 1.00000
DATE 2021 10 1.00000
DATE 2021 11 1.00000
DATE 2021 12 1.00000
DATE 2022 1 1.00000
DATE 2022 2 1.00000
DATE 2022 3 1.00000
DATE 2022 4 1.00000
DATE 2022 5 1.00000
DATE 2022 6 1.00000
DATE 2022 7 1.00000
DATE 2022 8 1.00000
DATE 2022 9 1.00000
DATE 2022 10 1.00000
DATE 2022 11 1.00000
DATE 2022 12 1.00000
DATE 2023 1 1.00000
DATE 2023 2 1.00000
DATE 2023 3 1.00000
DATE 2023 4 1.00000
DATE 2023 5 1.00000
DATE 2023 6 1.00000
DATE 2023 7 1.00000
DATE 2023 8 1.00000
DATE 2023 9 1.00000
DATE 2023 10 1.00000
DATE 2023 11 1.00000
DATE 2023 12 1.00000
DATE 2024 1 1.00000
DATE 2024 2 1.00000
DATE 2024 3 1.00000
DATE 2024 4 1.00000
DATE 2024 5 1.00000
DATE 2024 6 1.00000
DATE 2024 7 1.00000
DATE 2024 8 1.00000
DATE 2024 9 1.00000
DATE 2024 10 1.00000
DATE 2024 11 1.00000
DATE 2024 12 1.00000
DATE 2025 1 1.00000
DATE 2025 2 1.00000

DATE 2025 3 1.00000
DATE 2025 4 1.00000
DATE 2025 5 1.00000
DATE 2025 6 1.00000
DATE 2025 7 1.00000
DATE 2025 8 1.00000
DATE 2025 9 1.00000
DATE 2025 10 1.00000
DATE 2025 11 1.00000
DATE 2025 12 1.00000
DATE 2026 1 1.00000
DATE 2026 2 1.00000
DATE 2026 3 1.00000
DATE 2026 4 1.00000
DATE 2026 5 1.00000
DATE 2026 6 1.00000
DATE 2026 7 1.00000
DATE 2026 8 1.00000
DATE 2026 9 1.00000
DATE 2026 10 1.00000
DATE 2026 11 1.00000
DATE 2026 12 1.00000
DATE 2027 1 1.00000
DATE 2027 2 1.00000
DATE 2027 3 1.00000
DATE 2027 4 1.00000
DATE 2027 5 1.00000
DATE 2027 6 1.00000
DATE 2027 7 1.00000
DATE 2027 8 1.00000
DATE 2027 9 1.00000
DATE 2027 10 1.00000
DATE 2027 11 1.00000
DATE 2027 12 1.00000
DATE 2028 1 1.00000
DATE 2028 2 1.00000
DATE 2028 3 1.00000
DATE 2028 4 1.00000
DATE 2028 5 1.00000
DATE 2028 6 1.00000
DATE 2028 7 1.00000
DATE 2028 8 1.00000
DATE 2028 9 1.00000
DATE 2028 10 1.00000

DATE 2028 11 1.00000
DATE 2028 12 1.00000
DATE 2029 1 1.00000
DATE 2029 2 1.00000
DATE 2029 3 1.00000
DATE 2029 4 1.00000
DATE 2029 5 1.00000
DATE 2029 6 1.00000
DATE 2029 7 1.00000
DATE 2029 8 1.00000
DATE 2029 9 1.00000
DATE 2029 10 1.00000
DATE 2029 11 1.00000
DATE 2029 12 1.00000
DATE 2030 1 1.00000
DATE 2030 2 1.00000
DATE 2030 3 1.00000
DATE 2030 4 1.00000
DATE 2030 5 1.00000
DATE 2030 6 1.00000
DATE 2030 7 1.00000
DATE 2030 8 1.00000
DATE 2030 9 1.00000
DATE 2030 10 1.00000
DATE 2030 11 1.00000
DATE 2030 12 1.00000
DATE 2031 1 1.00000
DATE 2031 2 1.00000
DATE 2031 3 1.00000
DATE 2031 4 1.00000
DATE 2031 5 1.00000
DATE 2031 6 1.00000
DATE 2031 7 1.00000
DATE 2031 8 1.00000
DATE 2031 9 1.00000
DATE 2031 10 1.00000
DATE 2031 11 1.00000
DATE 2031 12 1.00000
DATE 2032 1 1.00000
DATE 2032 2 1.00000
DATE 2032 3 1.00000
DATE 2032 4 1.00000
DATE 2032 5 1.00000
DATE 2032 6 1.00000

DATE 2032 7 1.00000
DATE 2032 8 1.00000
DATE 2032 9 1.00000
DATE 2032 10 1.00000
DATE 2032 11 1.00000
DATE 2032 12 1.00000
DATE 2033 1 1.00000
DATE 2033 2 1.00000
DATE 2033 3 1.00000
DATE 2033 4 1.00000
DATE 2033 5 1.00000
DATE 2033 6 1.00000
DATE 2033 7 1.00000
DATE 2033 8 1.00000
DATE 2033 9 1.00000
DATE 2033 10 1.00000
DATE 2033 11 1.00000
DATE 2033 12 1.00000
DATE 2034 1 1.00000
DATE 2034 2 1.00000
DATE 2034 3 1.00000
DATE 2034 4 1.00000
DATE 2034 5 1.00000
DATE 2034 6 1.00000
DATE 2034 7 1.00000
DATE 2034 8 1.00000
DATE 2034 9 1.00000
DATE 2034 10 1.00000
DATE 2034 11 1.00000
DATE 2034 12 1.00000
DATE 2035 1 1.00000
DATE 2035 2 1.00000
DATE 2035 3 1.00000
DATE 2035 4 1.00000
DATE 2035 5 1.00000
DATE 2035 6 1.00000
DATE 2035 7 1.00000
DATE 2035 8 1.00000
DATE 2035 9 1.00000
DATE 2035 10 1.00000
DATE 2035 11 1.00000
DATE 2035 12 1.00000
DATE 2036 1 1.00000
DATE 2036 2 1.00000

DATE 2036 3 1.00000
DATE 2036 4 1.00000
DATE 2036 5 1.00000
DATE 2036 6 1.00000
DATE 2036 7 1.00000
DATE 2036 8 1.00000
DATE 2036 9 1.00000
DATE 2036 10 1.00000
DATE 2036 11 1.00000
DATE 2036 12 1.00000
DATE 2037 1 1.00000
DATE 2037 2 1.00000
DATE 2037 3 1.00000
DATE 2037 4 1.00000
DATE 2037 5 1.00000
DATE 2037 6 1.00000
DATE 2037 7 1.00000
DATE 2037 8 1.00000
DATE 2037 9 1.00000
DATE 2037 10 1.00000
DATE 2037 11 1.00000
DATE 2037 12 1.00000
DATE 2038 1 1.00000
DATE 2038 2 1.00000
DATE 2038 3 1.00000
DATE 2038 4 1.00000
DATE 2038 5 1.00000
DATE 2038 6 1.00000
DATE 2038 7 1.00000
DATE 2038 8 1.00000
DATE 2038 9 1.00000
DATE 2038 10 1.00000
DATE 2038 11 1.00000
DATE 2038 12 1.00000
DATE 2039 1 1.00000
DATE 2039 2 1.00000
DATE 2039 3 1.00000
DATE 2039 4 1.00000
DATE 2039 5 1.00000
DATE 2039 6 1.00000
DATE 2039 7 1.00000
DATE 2039 8 1.00000
DATE 2039 9 1.00000
DATE 2039 10 1.00000

DATE 2039 11 1.00000
DATE 2039 12 1.00000
DATE 2040 1 1.00000
STOP

VITA

Name:	Anish Singh Chaudhary
Address:	EOG Resources Inc., 3817 NW Expressway #500, Oklahoma City, Ok 73112
Email Address:	anish.petro@gmail.com
Education:	B.Tech., Petroleum Engineering, Indian School of Mines, 2002 M.S., Petroleum Engineering, Texas A&M University, 2011